JGR Atmospheres

RESEARCH ARTICLE
10.1029/2024JD042254

The Impact of the 2023 Canadian Forest Fires on Air Quality in Southern Ontario

Victoria A. Flood[1], Kimberly Strong[1], Cynthia H. Whaley[2], Jack Chen[3], Debra Wunch[1], James R. Drummond[4], Orfeo Colebatch[1], Lawson Gillespie[1], and Nasrin Mostafavi Pak[1,5]

[1]Department of Physics, University of Toronto, Toronto, ON, Canada, [2]Canadian Centre for Climate Modelling and Analysis, Environment and Climate Change Canada, Victoria, BC, Canada, [3]Air Quality Research Division, Environment and Climate Change Canada, Ottawa, ON, Canada, [4]Department of Physics & Atmospheric Science, Dalhousie University, Halifax, NS, Canada, [5]Now at: Institute of Meteorology and Climate Research Atmospheric Environmental Research (IMK-IFU), Karlsruhe Institute of Technology (KIT), Garmisch-Partenkirchen, Germany

Key Points:

- Extreme wildfire events in Canada caused poor air quality in Southern Ontario during the summer of 2023
- Enhancements in tropospheric CO, C_2H_6, CH_3OH, HCN and HCOOH from transported wildfire plumes were measured in Toronto and Egbert, Ontario
- GEM-MACH FireWork simulates the timing and spatial distribution of fire plumes well, but exhibits some biases in CO, NH_3, O_3, and $PM_{2.5}$

Correspondence to:
V. A. Flood,
v.flood@utoronto.ca

Citation:
Flood, V. A., Strong, K., Whaley, C. H., Chen, J., Wunch, D., Drummond, J. R., et al. (2025). The impact of the 2023 Canadian forest fires on air quality in Southern Ontario. *Journal of Geophysical Research: Atmospheres*, *130*, e2024JD042254. https://doi.org/10.1029/2024JD042254

Received 21 AUG 2024
Accepted 14 JAN 2025

Abstract The record-breaking 2023 Canadian wildfire season had large-scale burning that resulted in wide-reaching long-range transport of smoke plumes and their associated trace gases. This paper examines three events (May 16-23, June 3-9 and June 17-30, 2023) during which the composition of smoke was measured over Toronto and Egbert, Ontario. Tropospheric columns (0–10 km) of CO, C_2H_6, CH_3OH, HCN, HCOOH, NH_3 and O_3 were measured using high-resolution Fourier transform infrared spectrometers. Coincident enhancements of CO and other gases during the events were used to calculate enhancement ratios. Correlations with CO were observed for C_2H_6, CH_3OH, HCN and HCOOH, but not for NH_3 and O_3. Plume transport was investigated with the Hybrid Single-Particle Lagrangian Integrated Trajectory model, the GEM-MACH-FireWork (GM-FW) air quality model, and Measurements of Pollution in the Troposphere (MOPITT) CO satellite data. Additional measurements examined were surface CO, O_3, and $PM_{2.5}$, plume height from a Mini Micro Pulse Lidar, and EM27/SUN XCO columns. GM-FW model output was compared with ground-based surface and 0–10 km column measurements, and MOPITT CO maps. Over the 2023 forest fire season (May-September), the model underestimated background tropospheric columns of CO, NH_3 and O_3, but generally overestimated enhancements during smoke events. Relative to surface in situ measurements, GM-FW seasonal averages overestimated CO and underestimated O_3 (which was not generally enhanced during smoke events), while $PM_{2.5}$ fluctuated between a positive and negative bias. Compared to MOPITT, the GM-FW event-averaged CO columns appropriately represent plume dispersion across the country, with some offsets on the scale of the ground-based locations that are consistent with the discussed findings.

Plain Language Summary Intense wildfires in Canada during the summer of 2023 resulted in widespread smoke and poor air quality downwind. Air pollution related to the smoke was measured in Toronto and Egbert, Ontario. Based on these measurements, three main air pollution episodes are investigated: May 16-23, June 3-9 and June 17-30. Model simulations of these events were evaluated and also used as a tool to show that air passed over various active fire regions right before these poor air quality events. The models and measurements allow us to quantify the amount of pollution that came from long-range transport of fire emissions.

1. Introduction

The summer of 2023 marked an unprecedented year for wildfires in Canada. The burned area surpassed 16 million hectares, which is more than the cumulative total burned area from the previous eight years (2015–2022) (CWFIS, 2024). The National Oceanic and Atmospheric Administration (NOAA) 2023 Annual Climate Report indicates that 2023 was the hottest year on record, both globally and for North America (NOAA, 2024). The 2023 fire season was unique for Canada: it started in late April, which is earlier than normal, and persisted into October (Jain et al., 2024). Sizable wildfire events, such as those occurring in 2023, can have significant implications for local ecosystems, human health, and the economy.

A study by the Great Lakes Forestry Center reviewing fire trends in Canada from 1959 to 2015 shows a significant increase in burned area over time, dominated by large fires, which were found to have doubled over the study period (Hanes et al., 2019). The Fire Weather Index (FWI) is a rating used to represent the "fire danger" of a region, encompassing temperature, humidity, wind, and precipitation (Van Wagner, 1987). Approximately half of

the forest fires in Canada are attributed to ignition by lightning, although they account for the majority of the burned area (Hanes et al., 2019). In 2023, dry conditions resulting from early snowmelt and an extended period of drought, in addition to the high-temperature anomalies, contributed to an increased FWI. Jones et al. (2022) highlight a relationship between burned area and FWI in Canada, stating that models that use FWI as an indicator for future fire activity project an increase due to anthropogenic climate change. Furthermore, fire management policies in Canada involving fire suppression have resulted in an amplified risk of wildfires by increasing the flammability in the boreal wildland-urban interface (Parisien et al., 2020).

Over 5,000 air quality alert bulletins were issued by Environment and Climate Change Canada (ECCC) in 2023, compared to the national annual average of 1,300 from 2017 to 2022 (Jain et al., 2024). In Canada, wildfire-$PM_{2.5}$ for 2013–2015 and 2017–2018 is estimated to have caused 54–240 premature deaths due to short-term exposure, and 570–2,500 premature deaths from long-term exposure, along with several other adverse health outcomes (Matz et al., 2020). The five-year total (2013–2018) economic impact of the wildfire-$PM_{2.5}$, as it relates to health, was predicted to be $49 billion (CAD). During the summer of 2023, some of the worst-affected areas of Canada had more than 60 days with poor air quality due to wildfire-related pollution (Jain et al., 2024). Negative health impacts are more significant to communities closer to the fire-affected areas; however, as fires continue to increase in frequency and size, exposure rates both locally and via long-range transport will rise. Although Southern Ontario does not generally experience wildfires, the area is densely populated, with ∼7 million people, or 18% of Canada's population, living in the Greater Toronto and Hamilton Area (Statistics Canada, 2023) and is susceptible to long-range transport of emissions from sizable wildfire events, as observed in the summer of 2023.

Chemical species released during biomass burning events can lead to degraded air quality and affect the climate and carbon cycle. Long-lived species are useful for tracking plumes and can provide information about the source biomass burning event. Yamanouchi et al. (2020) examined the long-range transport of trace gases related to fire emissions in the Toronto area using ground-based Fourier transform infrared (FTIR) spectroscopy. Using data from 2002 to 2018, the study found enhancements of carbon monoxide (CO), ethane (C_2H_6), methanol (CH_3OH), hydrogen cyanide (HCN), and formic acid (HCOOH) related to boreal and temperate forest fires. Similarly, enhancements of CO, HCN, C_2H_6, ammonia (NH_3), peroxyacetyl nitrate (PAN), ethylene (C_2H_4), CH_3OH and HCOOH were detected with an FTIR in the Canadian High Arctic, and attributed to fires in British Columbia and the Northwest Territories of Canada in 2017 (Lutsch et al., 2020; Wizenberg et al., 2023).

Generally speaking, estimates of fire emissions and transport dispersion models have key areas for improvement, including plume height parameterizations, vegetation type, fire type representations, plume chemistry and atmospheric transport (e.g., wind, precipitation, temperature), all of which may be confounded when fire plumes from several events are reaching one location at the same time. Chemical transport models which include fire emissions and simulate atmospheric processes, including chemistry, are applied operationally for emergency response and public health purposes, and as such it is important to work toward improvements of the models. A key step in this process is to evaluate models with observational data. The prolonged, large-spread smoke events that occurred in the summer of 2023 across Canada, and the subsequent atmospheric measurements, provide an opportunity to test the performance of the models.

This study aims to evaluate the impact of the 2023 Canadian wildfires on the atmospheric composition and air quality in Southern Ontario through the amalgamation of data from several ground-based and satellite atmospheric monitoring instruments, a chemical transport model, and a back-trajectory model. The transport of wildfire smoke is evaluated through its related trace gases using measurements from high-resolution, ground-based FTIR spectrometers, located in Toronto and Egbert, Ontario. This method is capable of simultaneously measuring several atmospheric trace gases, to provide information about the composition of the smoke plume. Additionally, CO measurements are supplemented with total column CO from a lower-resolution FTIR instrument at the University of Toronto and from the Measurements of Pollution in the Troposphere (MOPITT) satellite instrument. Smoke plume heights are assessed with a Mini Micro Pulse Lidar (MiniMPL) instrument, and trajectories are estimated using the Hybrid Single-Particle Lagrangian Integrated Trajectory (HYSPLIT) dispersion model. Surface concentrations of CO, O_3 and $PM_{2.5}$ from the Ontario Ministry of Environment, Conservation and Parks (OMECP) are discussed in relation to air quality during these events. The GEM-MACH FireWork (GM-FW) air quality forecast model outputs are evaluated against tropospheric partial columns of CO, NH_3 and O_3, local surface measurements of CO, O_3 and $PM_{2.5}$, and mapped satellite total column CO. The paper is structured

as follows: Section 2 describes the datasets used, Section 3 outlines the methodology, Section 4 presents results and discussion, and Section 5 provides a summary and conclusions.

2. Datasets

2.1. Fourier Transform Infrared Spectroscopy Measurements

Solar-viewing FTIR spectrometers are used to record solar absorption spectra from which trace gas profiles and columns are retrieved. The method requires sunny days with relatively low cloud/haze to operate, which leads to intermittent gaps in the measurements. Unless otherwise stated, the use of "FTIR" (data/measurements) refers to the high-resolution FTIR instruments described in Section 2.1.1, while data from the lower-resolution EM27/SUN FTIR will be specified as such.

2.1.1. High-Resolution

Two ABB Bomem DA8 FTIR spectrometers are used in this work: one is located at the University of Toronto Atmospheric Observatory (TAO) in downtown Toronto (43.66°N, 79.4°W, 174 masl), and the other is located at ECCC's Centre for Atmospheric Research Experiments (CARE) in Egbert (44.23°N, 79.78°W, 251 masl). The instrument locations are shown in Figure 1, where the yellow 'x' marks CARE and orange '+' marks TAO. The instruments have a 250 cm optical path difference, which produces a spectral resolution of 0.004 cm^{-1}. The instruments record solar absorption spectra optimized for different atmospheric gases by cycling through a series of filters covering spectral ranges between 650 and 4,500 cm^{-1}. Using the optimal estimation method, trace gas profiles and column densities are retrieved with the SFIT4 algorithm (IRWG, 2020; Rodgers, 2000). The program uses temperature and pressure profiles from the U.S. National Centers for Environmental Prediction (Kalnay et al., 1996), a priori trace gas profiles from Whole Atmosphere Community Climate Model v4 (Marsh et al., 2013) and spectroscopic absorption parameters from the HITRAN 2008 line-list (Rothman et al., 2009).

The TAO FTIR has been operational since 2002 and is a member of the Network for the Detection of Atmospheric Composition Change (NDACC) (De Mazière et al., 2018). The CARE FTIR began measurements in 1996, operated intermittently until 2010, and started routine operations in spring 2023 (Whaley et al., 2013). The FTIR measurements examined in this paper are CO, C_2H_6, CH_3OH, HCN, HCOOH, NH_3 and O_3 (Yamanouchi et al., 2023). The daily mean CO tropospheric columns are well-correlated ($R = 0.85$) between the TAO and CARE sites. The TAO 2002–2023 0–10, 10–20 km partial column, and total column volume mixing ratio (VMR) averaging kernels (AVKs) for each of these species are shown in Figure 2, providing information about the contributions of the different altitudes to the retrieved columns. The trace of the AVK matrix provides the degrees of freedom for signal (DOFS), which indicates the number of independent pieces of information coming from the retrieval. Table 1 lists the mean percent uncertainty, and mean DOFS of the 0–10 km partial column, and total column DOFS for the gases of interest, using the entire TAO time series. The mean percent error is calculated from the sum of squares of the average random and systematic uncertainty of all years (following Vigouroux et al., 2009).

2.1.2. EM27/SUN

The EM27/SUN FTIR used in this study is located at the University of Toronto (UofT), co-located with the TAO FTIR (TAO "+" marker in Figure 1). This instrument uses a retrieval software called "GGG" to obtain column-averaged dry-air mole fractions (X_{gas}) of several species, including CO, CO_2, and CH_4 (Hedelius & Wennberg, 2023). The instrument is designed to be a portable solar-viewing Fourier transform spectrometer with a 1.8 cm optical path difference and a spectral resolution of 0.5 cm^{-1}, with a spectral range of 6,000–9,000 cm^{-1} (Gisi et al., 2012). One scan takes approximately 6 s, allowing for a more frequent product compared to the DA8 FTIR, which takes about 12 min. The XCO total column measurements are used here to supplement the CO measurements made by the higher-spectral-resolution FTIR data described above.

2.2. Air Quality Data

The OMECP partners with ECCC to provide hourly concentrations of pollutants and an Air Quality Health Index (AQHI) at 38 ambient air monitoring stations across the province (OMECP, 2024). Surface measurements for CO, O_3, and $PM_{2.5}$, and the AQHI are acquired for May through September 2023 for locations in Toronto and

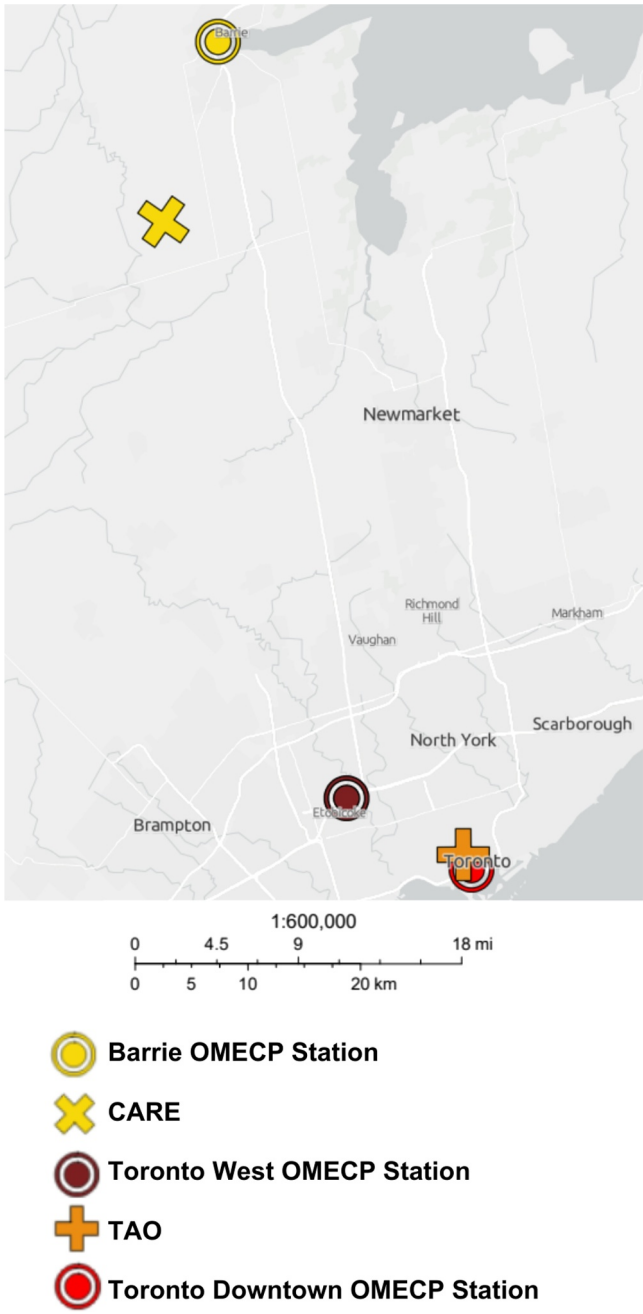

Figure 1. Map showing the locations of the ground-based instruments used in this paper (Esri, 2024).

Barrie (closest OMECP station to Egbert). The manufacturer's instrument detection limits are 0.04 ppm for CO, 0.5 ppb for O_3, and 0.5 $\mu g/m^{-3}$ for $PM_{2.5}$ at the Toronto Downtown location, and 0.1 $\mu g/m^{-3}$ for $PM_{2.5}$ at the Barrie location (Teledyne Advanced Pollution Instrumentation, 2016; Thermo Fisher Scientific, 2013, 2017a, 2017b). Note that only the "Toronto West" location provides CO measurements. The circles in Figure 1 show the OMECP station locations, where Barrie is in yellow (~18 km from CARE), Toronto West (~13 km from TAO) is in maroon, and Toronto Downtown is in red (~2 km from TAO). The daily mean values for $PM_{2.5}$ between the Toronto Downtown and Barrie locations are well correlated ($R = 0.90$).

2.3. Measurements of Pollution in the Troposphere

The MOPITT instrument is on NASA's Terra satellite, launched in 1999, and is operated by the Canadian Space Agency (CSA). It measures CO, focusing on the lower atmosphere, via a nadir-viewing infrared radiometer, covering 82°S to 82°N (Drummond et al., 1995). The satellite has an overpass time of 10:30/22:30 local time, and provides CO as a total column average in ppb. Validation using aircraft profiles shows that retrieval biases are on the order of ±5% (Deeter et al., 2022). The mean total column over the event periods of interest are mapped to provide large-scale context of the extent of the CO enhancements and used to assess the GEM-MACH-Firework CO long-range transport (NASA/LARC/SD/ASDC, 2024).

2.4. Mini Micro Pulse Lidar

The Micro Pulse Lidar Network (MPLNET) is a global network of ground-based lidar instruments that measures aerosol and cloud vertical profiles in support of the NASA Earth Observation System program (Campbell et al., 2002). The MiniMPL instrument located at the University of Toronto contributes measurements to MPLNET (TAO "+" marker in Figure 1). It samples the atmosphere every 60 s up to 15 km, and operates during daylight hours from sunrise to sunset. The data product used here is the Normalized Relative Backscatter (NRB), which is a relative lidar signal strength, in MHz km^2 μJ^{-1}; this is used to represent the approximate height of transported smoke layers (NASA, 2024).

2.5. Hybrid Single-Particle Lagrangian Integrated Trajectory Model

The HYSPLIT model is used to compute air parcel trajectories, dispersion, transport, deposition and transformation (Draxler & Hess, 1998; Stein et al., 2015). A primary feature of the program is the ability to simulate back-trajectories used for source-receptor relationship studies. In the context of smoke plumes, the program can be used to calculate source dispersion from the point of the fire (e.g., Li et al., 2020) or to calculate back-trajectories to investigate the sources contributing to air concentrations at a particular receptor location (e.g., Selimovic et al., 2019). Furthermore, HYSPLIT is used for the operational smoke forecasting system at NOAA to produce 48 hr smoke transport and concentration predictions (Stein et al., 2009), and for the United States Forest Service ensemble trajectories (USFS, 2024).

The HYSPLIT model offers a user-friendly online version called Real-time Environmental Applications and Display SYstem (READY) (Rolph et al., 2017). This allows a user to choose a location, height, meteorology, and timeframe to run trajectory dispersion simulations forwards or backwards in time. The air parcel trajectories move a single Lagrangian particle with the mean wind from the user-defined meteorological scheme, in this case the Global Data Assimilation System (GDAS) meteorology on 1° latitude-longitude grid with 23 pressure levels, and at 3 hr intervals. Errors in the trajectory arise from uncertainties in the input data such as

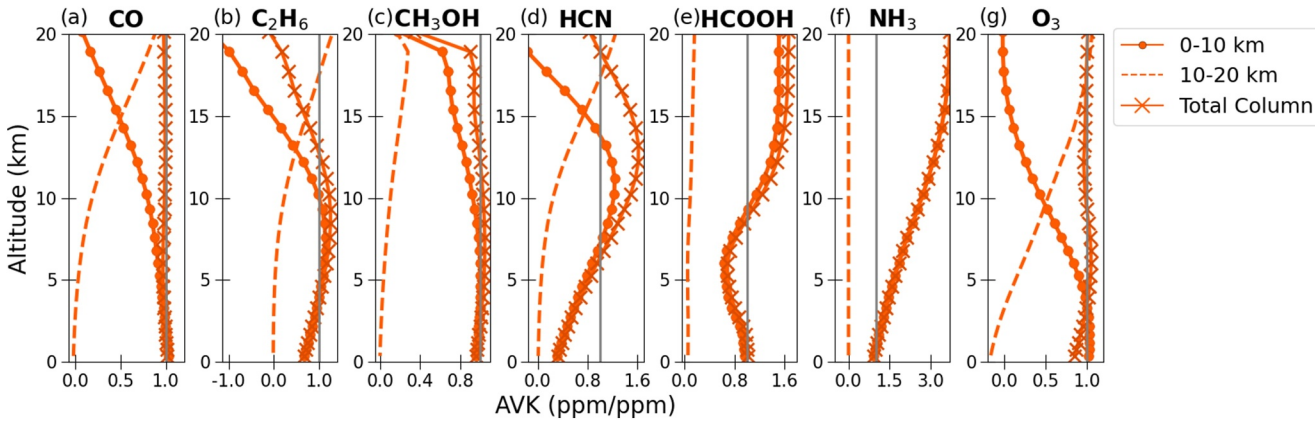

Figure 2. Mean 2002–2023 averaging kernels from the University of Toronto Atmospheric Observatory for 0–10 km (round markers) and 10–20 km (dashed line) partial columns, and for total columns shown for 0–20 km ('X' markers), with a gray line marking 1.

the forecast meteorology and representation of the atmosphere through space and time, in addition to computational errors, which in total are estimated to account for 15%–30% of the travel distance (Draxler & Rolph, 2007).

There are four options for the trajectory simulations: standard, matrix, ensemble or frequency. In the current application, the ensemble type was used, which starts 27 individual trajectories from the same location, with the initial calculation of the meteorological grid offset by ±1 grid point in the horizontal direction and 0.01 sigma units in the vertical. Using an ensemble of trajectories in the area of interest allows for a better approximation of the true state. Because uncertainties accumulate as a result of initial conditions in the trajectory calculation, running the ensemble simulation gives more confidence in the trajectory of air into a region in comparison to a single trajectory (Draxler, 2003). Running this program with back-trajectories allows for an assessment of air mass source areas for plumes that reached the location on a given date.

2.6. GEM-MACH-FireWork

Environment and climate change Canada produces a near-term operational regional air quality forecast called the Regional Air Quality Deterministic Prediction System (RAQDPS). This is used to generate local AQHI forecasts based on model-predicted surface concentrations of O_3, $PM_{2.5}$ and NO_2 pollutants (Chen & GEM-MACH development team, 2019). Underlying this system is the chemical transport model GEM-MACH (Global Environmental Multi-scale Modeling Air quality and Chemistry). FireWork is an extension of the RAQDPS with the same anthropogenic emissions, grid, meteorology, and boundary conditions but with the addition of near-real-time biomass-burning emissions (Chen et al., 2019; Pavlovic et al., 2016). The wildfire locations from the previous 24 hr are obtained from the Canadian Forest Services operational Canadian Wildland Fire Information System (CWFIS), using satellite hotspot data. Fire emissions are estimated using the Canadian Forest Fire

Table 1
Mean 2002–2023 University of Toronto Atmospheric Observatory 0–10 km Partial Column Percent Uncertainty, Degrees of Freedom for Signal (DOFS), and Total Column DOFS for Species of Interest

Gas	0–10 km partial column percent uncertainty	Mean total column DOFS ±1σ	Mean 0–10 km partial column DOFS ±1σ
CO	3.52	2.20 ± 0.25	1.69 ± 0.12
C_2H_6	4.90	1.88 ± 0.29	1.36 ± 0.19
CH_3OH	16.5	1.51 ± 0.15	1.37 ± 0.12
HCN	7.99	2.11 ± 0.40	0.82 ± 0.14
HCOOH	13.1	1.06 ± 0.04	0.93 ± 0.02
NH_3	15.4	1.11 ± 0.09	1.11 ± 0.09
O_3	6.28	4.38 ± 0.52	1.11 ± 0.18

Emission Prediction System (CFFEPS) accounting for fire behavior and regional meteorology (Chen et al., 2019). This allows for model simulations over the North American domain on a 10 × 10 km grid, with and without fire emissions. Fire plume height is determined by the thermodynamic plume rise scheme in CFFEPS. When compared with satellite observations from the Multi-angle Imaging SpectroRadiometer (MIRS) and the TROPOspheric Monitoring Instrument (TROPOMI), on average, the GM-FW fire plume heights were above the observation by approximately 60–320 and 270–580 m, respectively (Griffin et al., 2020), although this is within the uncertainty range of these measurements. GM-FW fire emissions were compared to well-established global fire emissions inventories regionally and globally for the years 2015–2020, and were found to be within the range of these datasets, indicating that the modeled fire emissions should be realistic (Anderson et al., 2024).

The output includes three-dimensional fields of VMRs for several chemical species. Here, vertical profiles of CO, NH_3 and O_3 over downtown Toronto and Egbert are extracted from the simulations with and without fire emissions and used to derive columns as described in Section 3.3. Surface values for CO, O_3, and $PM_{2.5}$ are extracted from the area corresponding to the OMECP locations of Toronto Downtown, Barrie, and Toronto West (for CO). The mean total column CO over the period of the three events is mapped over the area of Canada, and compared to MOPITT CO over the same time. Hereafter, these model results will be referred to as GM-FW (all emissions) or GM (without fire emissions). The data version used in these comparisons corresponds to "024" where GM is "RAQDPS024" and GM-FW is "RAQDPSFW024" (ECCC, 2024).

2.7. Fire Perimeters

The fire perimeters used here are provided by the CWFIS Datamart (CWFIS, 2024). The hotspot locations are identified with satellite imagery from multiple sources, including the Advanced Very High-Resolution Radiometer (AVHRR) from the NOAA National Environmental Satellite, Data and Information Service (NESDIS), and NASA's Moderate Resolution Imaging Spectroradiometer (MODIS) and Visible Infrared Imaging Radiometer Suite (VIIRS). These are processed into mapped areas with inputs from fire management, fire weather/fire danger rating systems.

3. Methods

3.1. Defining Enhancements and Events

Trace gas enhancements in the 0–10 km TAO FTIR partial columns are identified relative to the historical monthly means. These monthly means are derived from the full TAO time series (2002–2022), labeled in Figure 3 as the baseline ("BL"). Given the extended gap in the FTIR operations at CARE, the TAO baseline is used for both locations. Enhancement events are defined as a period for which CO is (generally) above the 1σ standard deviation of the monthly mean. The baseline is used to calculate the relative percent enhancements during different events in Section 4. Figure 3a shows the 0–10 km partial column time series of the TAO (orange markers) and CARE (yellow markers) FTIR measurements, and the baseline (black line) with ±1σ (gray shading). These are supplemented with measurements from the EM27/SUN FTIR (Figure 3b) co-located with TAO. Figure 3c shows the OMECP surface hourly $PM_{2.5}$ measurements from Toronto and Barrie, along with the 2020 Canadian Ambient Air Quality Standard (CAAQS) for $PM_{2.5}$ marked in red (27 μg/m^{-3} over 24 hr mean) (Health Canada, 2023). Several enhancements of CO can be seen throughout the summer, and three events of interest (May 16-23, June 3-9, and June 17-30) are highlighted in the figure with light blue shading; these events are discussed in detail in Section 4. Similar to Figure 3a (and Figures A1-A6 in Appendix A) show the time series for 2023 of the other species discussed.

To compute enhancement ratios between the fire-related species (as listed in Table 1) and CO, a linear regression is applied to the "partial column enhancement" using all measurements within the defined events which occur within ±3 hr of a CO measurement (Lutsch et al., 2016; Yamanouchi et al., 2020). The partial column enhancement is expressed as the difference between the 0–10 km partial column measurement, and the monthly baseline (e.g., Paton-Walsh et al., 2005). As not every measurement within the events is enhanced, there are instances of negative values in these plots. The uncertainty of the enhancement ratio (slope) accounts for the errors in retrievals of both species (*x* and *y* axis) following the unified least squares approach in York et al. (2004).

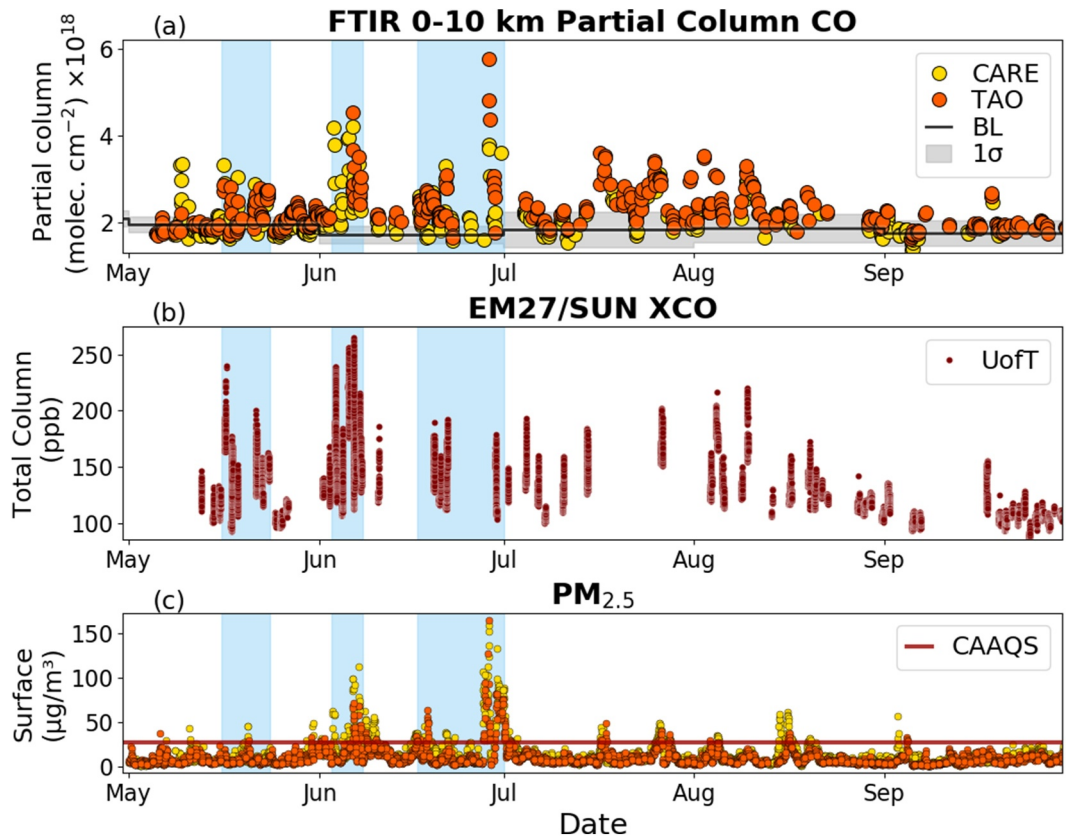

Figure 3. (a) CO 0–10 km partial columns from the University of Toronto Atmospheric Observatory (TAO) (orange) and Centre for Atmospheric Research Experiments (CARE) (yellow) Fourier transform infrared (FTIR) spectrometers, with the TAO monthly mean baseline (BL) ±1σ marked with a black line and gray shading, (b) UofT EM27/SUN XCO. (c) Ontario Ministry of Environment, Conservation and Parks $PM_{2.5}$ from Toronto (orange) and Barrie (yellow) with the Canadian Ambient Air Quality Standard (CAAQS) marked in red. The three events of interest are within the blue shaded regions.

3.2. Back-Trajectories

To determine the source of the air parcels transported over the TAO and CARE sites during the three events, the HYSPLIT ensemble trajectory model was used in the back trajectory simulation analysis. The times and dates of back-trajectories for each event were chosen based on when the CO enhancements, as measured by the high-resolution and EM27/SUN FTIRs (as shown in Figure 3), and OMECP hourly air quality reports were at their peak values (similar to Selimovic et al., 2019). The dates/times chosen were 20:00 UTC May 16 for Event 1, 19:00 UTC June 6 for Event 2, and 21:00 UTC June 28 for Event 3. The trajectories were calculated for 72 hr back from these air parcel arrival times.

To choose the heights for which the back-trajectories are released, the TAO FTIR and MiniMPL data were used to determine the presence of the smoke layer during each event. Figure 4 shows the percent difference between the measured profiles during the day selected for the back trajectory and the baseline profile to locate the altitudes of the peak relative enhancements. To supplement this, the MiniMPL NRB values corresponding to the same measurement time (within ±1 hr) were plotted as a function of altitude. In the FTIR profiles, there are maxima in the differences profile (Figures 4a–4c) at approximately 5 km for Event 1, and 1 km for Events 2 and 3. These correspond well with the peak NRBs observed by the MiniMPL (Figures 4d–4f) for those events, which are at higher vertical resolution than the FTIR data (note that the MiniMPL points above the fire enhancements are a result of noise from signal attenuation from above the smoke layer). Based on these profiles, the HYSPLIT ensemble back-trajectories were released from 1,000 to 5,000 m, which corresponds to the peak CO and NRB profiles for the three events.

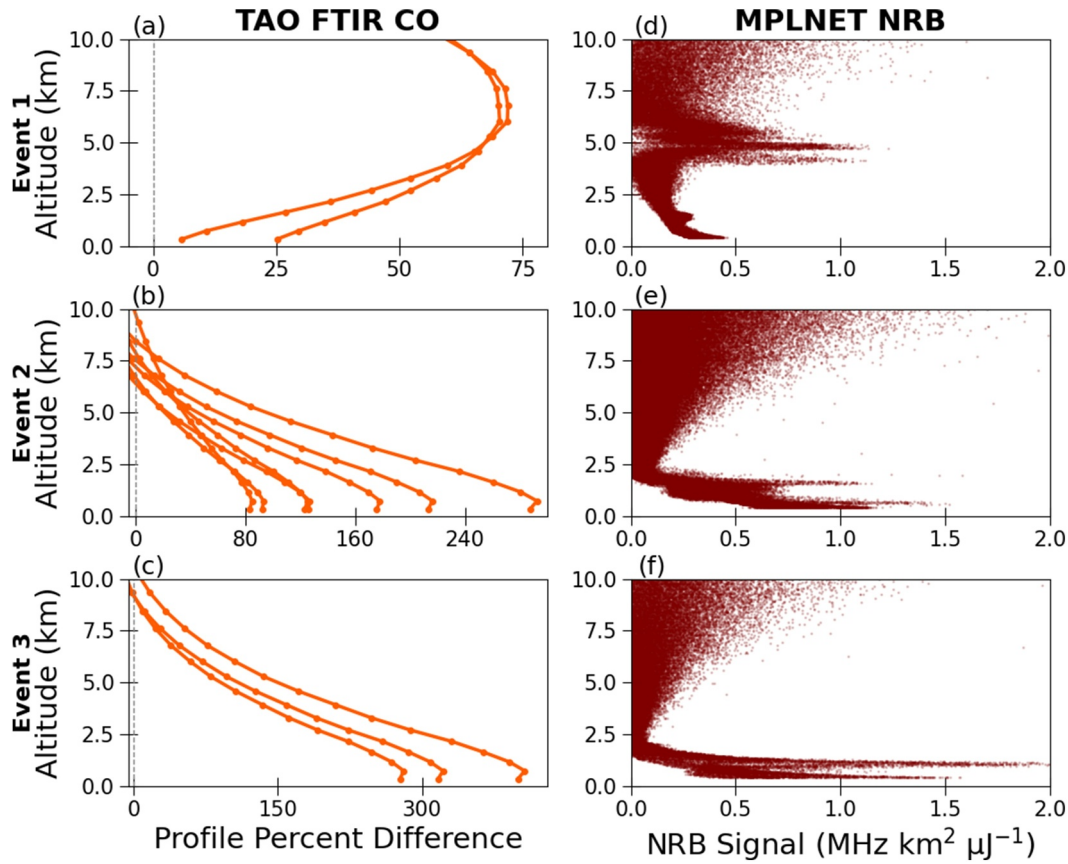

Figure 4. (a–c) University of Toronto Atmospheric Observatory (TAO) Fourier transform infrared (FTIR) spectrometer CO profile percent difference between the measurements on the peak day and the TAO baseline (100 × (meas. − mean)/mean), (d–f) UofT Mini Micro Pulse Lidar Network (MiniMPL) Normalized Relative Backscatter (NRB) for the times corresponding to FTIR measurements. Event 1 (a/d) shows May 16, Event 2 (b/e) shows June 6, and Event 3 (c/f) shows June 28.

3.3. GEM-MACH FireWork Comparisons

Model simulation results are available at one-hour intervals, so the FTIR measurements are matched with the output at the nearest hour. The FTIR and model data are aligned using the process outlined in Flood et al. (2024). Briefly, the modeled atmospheric profile is extracted corresponding to the geographic location closest to the FTIR instruments, interpolated onto the FTIR pressure grid, and smoothed with the corresponding AVK and a priori profile. The smoothed model output is converted from a VMR profile (in ppm) to a vertical profile in molecules cm^{-2}, and summed from 0 to 10 km to get partial columns.

These are used to evaluate how the GM-FW model simulates the tropospheric columns of CO, NH_3 and O_3, as compared to the high-resolution FTIR instruments at TAO and CARE. Using the GEM-MACH outputs with fire emissions ("GM-FW") versus without fire emissions ("GM") allows for the direct attribution and assessment of the impact of wildfires on atmospheric composition in the downwind receptor areas. The differences are assessed as a time series with the percent difference between GM-FW and the time-matched FTIR measurement, and overall percent difference (the mean of the percent differences) and the normalized root mean square error (NRMSE) (as described in Flood et al., 2024). In addition, the comparisons are presented in scatter plots, with a linear regression showing the slope and *R* value for both locations.

To assess the GM-FW vertical profiles, the mean profiles for each event are compared to the mean TAO FTIR profiles for each event. Additionally, the mean percent enhancement is calculated, similar to Figures 4a–4c, with the FTIR compared to the baseline profile, and GM-FW compared to GM to show where in the profile the enhancements are the most significant.

In addition to the partial columns and profiles, the GM-FW surface VMR of CO, O_3 and $PM_{2.5}$ are compared with the OMECP surface measurements from the Barrie and Toronto stations. As mentioned, CO is only available from Toronto West, and the closest OMECP location to Egbert is Barrie; for these, the model output is extracted for the closest possible grid point. As both the model and OMECP give hourly concentrations, the comparisons are made using daily averages to reduce the impact of outliers and diurnal cycles. Similarly these are shown as a time series with percent difference, overall mean percent difference, NRMSE, and as a scatter plot with a linear regression.

To evaluate plume location during the events, the event-averaged CO VMR from GM-FW is plotted on a map of Canada, and on a zoomed-in map of Southern Ontario for each event. Comparing these maps with the similar maps of event-averaged CO columns measured by MOPITT allows for an assessment of the CO spatial distribution during each event.

4. Results and Discussion

4.1. Long-Range Transport of Events

Three events were defined based on the enhancements as discussed above. The time marked as "Event 1" is from May 16 to 23, "Event 2" is from June 3 to 9, and "Event 3" is from June 17 to 30. Each event resulted in progressively worse air quality in Southern Ontario (see the AQHI from Toronto Downtown for each event in Table A1 and AQHI map in Figure A7). Toronto experienced a total of 14 "poor air quality" days during the summer of 2023, where the maximum single-day mean $PM_{2.5}$ reached 129 μg m^{-3} (during Event 3), almost 5 times the CAAQS (Health Canada, 2023; Jain et al., 2024). Mendez-Espinosa et al. (2019), found both a temporal and spatial coincidence between pollution levels (including CO and $PM_{2.5}$), fire location/frequency and air mass origin when using HYSPLIT back-trajectories to examine urban air quality with fires within a buffer zone. Here, the difference between events can be observed in both the size/number of active fires and the long-range transport that is incident on the region, as depicted by the HYSPLIT back-trajectories.

Figure 5 shows the HYSPLIT 72 hr ensemble back trajectory initiated at 5,000 m above ground level (magl) (a, c, e) and 1,000 magl (b, d, f) from TAO for Event 1 (a, b), Event 2 (c, d) and Event 3 (e, f). The color bar (blue to yellow) indicates the frequency at which air parcels from the ensemble passed over a given area, where a brighter yellow represents a higher occurrence. The red polygons represent the active fire hotspots at that time of the event with data from the CWFIS Datamart. The distance between TAO and CARE (70 km) is minimal compared to the distanced traveled by the air parcels as depicted in the back-trajectories; the CARE back-trajectories are comparable to these for TAO and are available in the Appendix (Figure A8).

Event 1 was an early season event, where fires were concentrated in Western Canada. Figures 5a and A8a show that the trajectories around 5 km in altitude during this time had passed over the fires in Alberta and Saskatchewan. The 1 km trajectories (Figures 5b and A8b) did not extend as far, but show some overpass of fires in the Prairies. During Event 1, the AQHI remained predominately at "low risk" in both Toronto and Barrie, but with enhanced tropospheric columns, indicating that smoke plumes were aloft in the area. According to the CWFIS hotspot report, approximately 9,506 km^2 were burned in Canada during Event 1 (CWFIS, 2024).

Event 2 happened as fire activity across Canada began to increase, particularly in Quebec. Figure 5c/d and Figure A8c/d show that at this time both the 1 and 5 km trajectories had traveled a similar path, crossing over fires in northwest Quebec. During this event, the AQHI in Southern Ontario was generally rated as "moderate risk", with surface VMRs above the CAAQS threshold, and partial columns greatly enhanced. According to the CWFIS hotspot report, approximately 13,153 km^2 were burned in Canada during Event 2 (CWFIS, 2024).

Event three exhibited the most severe air quality degradation in Southern Ontario region, with active fires in many areas across the country. Figures 5e and A8e show that the 5 km trajectories reached the region after passing over fires in Northern Alberta, Saskatchewan, Manitoba, and Northern Ontario. The 1 km trajectories (Figures 5f and A8f) can be seen passing over the large active fires in Quebec. At the peak of the smoke event, the AQHI in Barrie and Toronto was labeled as "high risk", smoke haze was visible to the eye and both surface and partial column measurements reached their local maximum for the year. According to the CWFIS hotspot report, approximately 24,659 km^2 were burned in Canada during Event 3 (CWFIS, 2024).

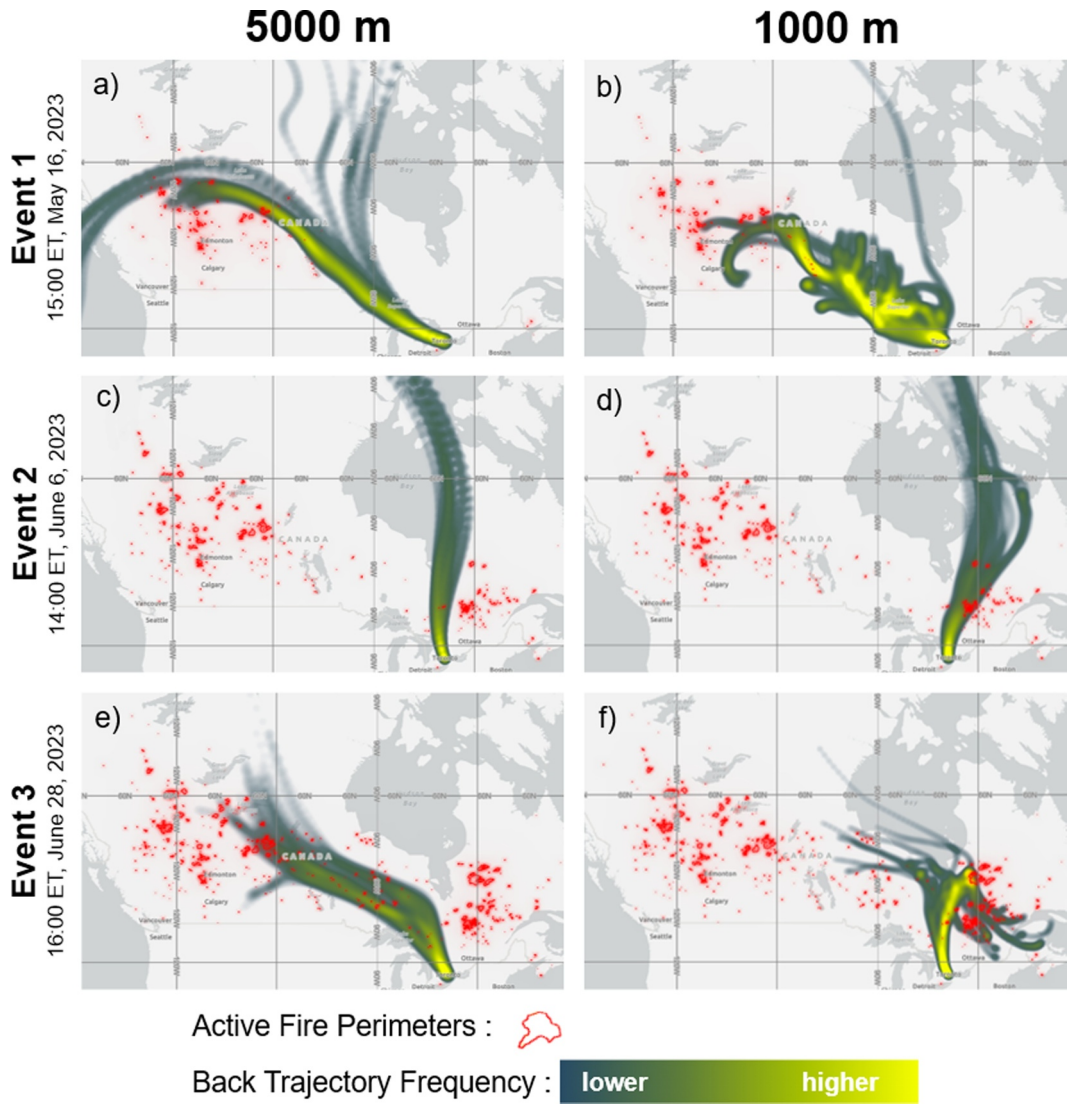

Figure 5. Hybrid Single-Particle Lagrangian Integrated Trajectory (HYSPLIT) 72 hr ensemble back-trajectories, initiated from the University of Toronto Atmospheric Observatory at the times listed, from 5,000 m (a,c,e) and 1,000 m (b,d,f). Red polygons represent the active fires at the time (CWFIS, 2024; Esri, 2020).

4.2. Enhancement Ratios

Enhancement ratios indicate the downwind relationship between a target species and a long-lived reference species (here CO) and provide insight into the composition of a plume. These relationships can be a useful reference point for developments in chemical transport models. As described in Section 3.1, the enhancement ratios are represented by the error-weighted linear regression of the partial column enhancements, during the events. Figure 6 shows the 0–10 km partial column enhancements between each gas and CO for May–September 2023 measured within 3 hr of each other for both TAO and CARE (gray). The times which correspond to measurements within the fire events are colored, and the rest of the measurements May–September 2023 are gray. The number of measurements for any given time is dependent on the operations of the FTIR, which may be restricted due to reduced solar intensity (e.g., weather, cloud, haze thick smoke) or operational downtimes. Due to the similarities shown in the long-range trajectories examined in Section 4.1 (Figures 5 and A8), the line of best fit and the consequent regression analysis is applied to the combination of CARE and TAO data, to maximize the number of data points used. To examine the differences between the fire events and their transport to Southern Ontario, the enhancement ratios for each event are plotted separately (Figure 6). Assuming that the major

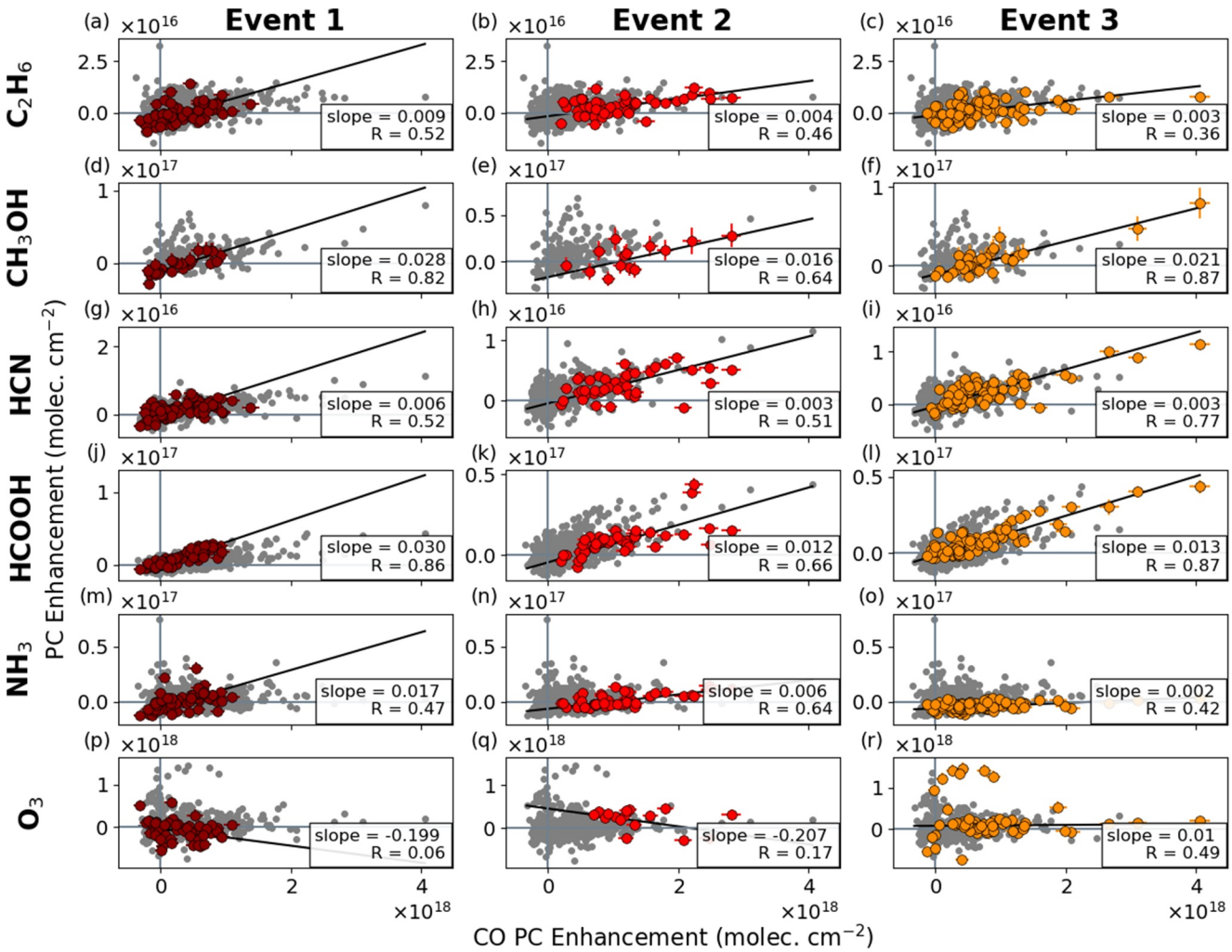

Figure 6. 0–10 km partial column (PC) enhancement of biomass-burning-related species versus CO (measured within ±3 hr) for the University of Toronto Atmospheric Observatory (TAO) and Centre for Atmospheric Research Experiments (CARE) Fourier transform infrared spectrometers from May - September 2023 (gray), with events marked by color, and separated by column. Error-weighted slopes are shown for the combined TAO and CARE datasets.

contributions throughout each event are represented by the HYSPLIT back-trajectories (Figures 5 and A8), Event 1 was due to transport from Western Canada, Event 2 from Quebec, and Event 3 a mix of both. Figure A9 in the Appendix shows the same information as Figure 6, but with data from the three events combined, and a single enhancement ratio calculated for each species. Table A3 summarizes the different slopes and *R* values between the two methods and indicates if the slope/R value increased (green shading), decreased (red shading) or remained the same (yellow shading) relative to the combined value.

A well-defined positive relationship is observed between enhancements in CO with C_2H_6 (R = 0.36–0.52), CH_3OH (R = 0.64–0.82), HCN (R = 0.51–0.77), and HCOOH (R = 0.66–0.87) during the events. The correlation between CO and NH_3 (R = 0.32–0.47) is lower, and even less so for O_3 (R = 0.06–0.49). There are fewer enhancements present in the time series for NH_3 and O_3 (as seen in Figures A5 and A6), which result in more partial column enhancements on or near the negative axes, and less correlation with the fire-enhanced CO values. This may be linked to NH_3's short lifetime with primarily agricultural sources in Southern Ontario, and O_3's non-linear photochemistry that may be suppressed during some fire events. The regression only considers points during the events, similar to other studies which examine enhancement ratios with FTIR measurements (e.g., Lutsch et al., 2016; Yamanouchi et al., 2020), where all observations within an event are used. However, the ratios presented here consider the partial column enhancements relative to the background level, rather than a total column measurement, as the previously mentioned studies do.

Comparing the 2023 enhancement ratios to those discussed in the long-term TAO analysis (Yamanouchi et al., 2020), C_2H_6 is within the broad range previously reported (0.003–0.009 vs. 0.0012–0.019), CH_3OH is generally lower (0.016–0.028 vs. 0.029–0.045), HCN is within the previously reported range (0.003–0.006 vs. 0.0037–0.0057), and HCOOH is also lower (0.012–0.030 vs. 0.033–0.041). When comparing with the combined values, with the exception of O_3, all of the enhancement ratios are increased with Event 1 (smoke from western Canada), decreased with Event 2 (smoke from Quebec), and are mixed for Event three (increased, decreased, and unchanged). The Event 1 values are closer to those reported in Yamanouchi et al. (2020), consistent with less intense, long-range transport more commonly experienced by the Toronto area. The differences in enhancement ratios between the three events may be due to differences in vegetation, burn phase, meteorology along the plume path, and/or chemistry and plume aging. All are particularly relevant for CH_3OH and HCOOH, which have a more significant difference in slopes and improved R-values when split, and are shorter-lived species (Jacob et al., 2005; Paulot et al., 2011). Species like C_2H_6 and HCN have somewhat higher R values when combined, and less significant slope changes, which is consistent with their longer chemical lifetimes and less dependence on plume aging over these distances and time scales (Viatte et al., 2013; Xiao et al., 2008). The higher R values and broad range in ratios between events for NH_3 and O_3 highlight the reactivity and variability of these species, which will be discussed further in the following paragraphs.

NH_3 was not discussed in respect to biomass burning enhancements with the TAO FTIR in Yamanouchi et al. (2020), however it was considered in Lutsch et al. (2016) in relation to the long-range transport of emissions from the 2017 fires in Northwest Territories, Canada. They report an enhancement ratio of 0.00465 with an R value of 0.45; here, the R value and slope are lower ($R = 0.34$ and 0.003). Additionally, the NH_3/CO correlation coefficient derived from the same 2017 fires are higher at the High Arctic site at Eureka (80°N) than at Toronto ($R = 0.70$ vs. $R = 0.45$), in part because of fewer local NH_3 sources (e.g., agricultural, urban, industrial) contributing to the signal in the Arctic. During the 2019 Fire Influence on Regional to Global Environments and Air Quality (FIREX-AQ) campaign, NH_3 and submicron particulate ammonium (NH_4^+) were measured with aircraft in smoke plumes. This showed that in wildfire plumes, NH_3 was converted to NH_4^+ within 2 hr of emission (Tomsche et al., 2023). Using aircraft measurements from the Western Wildfire Experiment for Cloud Chemistry, Aerosol Absorption, and Nitrogen (WE-CAN), Lindaas et al. (2021) studied NH_3 and NH_4 in fresh (<1 day) to old plumes (>3 days). They found that conversion to NH_4 increases NH_3 loss in fresh plumes; although background errors become larger as a plume dilutes and enhancements approach background levels. Adams et al. (2019) discuss the broad range of NH_3/CO emission factors, referencing a short (and method-dependent) lifetime (3–48 hr) and the association of NH_3 release during smoldering combustion. The combination of a short lifetime, reactivity, and variable local sources in Southern Ontario can all contribute to the lower correlation seen here.

Tropospheric ozone is a pollutant of concern to human health, which forms as a secondary product, through photochemical reactions of NOx and volatile organic carbons (VOCs) in the presence of sunlight. Its concentration resulting from wildfires also varies with properties such as plume height, burn characteristics, plume age, and meteorology (Jaffe & Wigder, 2012). The ratio of O_3/CO above a background value can indicate the O_3 production within a smoke plume, and has been found to have a wide range of values, including negative values (Jaffe & Wigder, 2012, and references therewithin). Ratios have been found to be higher in tropical/equatorial areas and increase with plume age, both of which are influenced by NOx availability (Jaffe & Wigder, 2012). Schneider et al. (2021) found that surface O_3 in Western Canada was both enhanced and reduced during wildfire events, remarking that pollutants present in urban areas can confound the ratios. A study of the intense 2016 Alberta boreal forest fires found no substantial increase in surface O_3 with downwind plumes aged approximately 0.5–2.5 days, citing unfavorable meteorological conditions for O_3 formation (Wentworth et al., 2018). All of these factors may contribute to the poor correlation observed between O_3 and CO in the TAO and CARE datasets with respect to the 2023 Canadian wildfires. Furthermore, the previous long-term analysis of wildfire emissions present in the TAO FTIR dataset did not discuss O_3 enhancements related to biomass burning (Yamanouchi et al., 2020). The surface O_3 measurements collected in Toronto and Barrie by OMECP during the summer of 2023 are quite variable, there are some instances where the values surpass the CAAQS standard (62 ppb, based on the 3 year average of the fourth-highest daily maximum), however these do not align with the events discussed in this paper (see Figure A10).

Zhang et al. (2024) used two satellite instruments, ACE-FTS (Atmospheric Chemistry Experiment—Fourier Transform Spectrometer) and OMPS LP (Ozone Mapping and Profile Suite Limb Profiler), to assess trace gas enhancements related to the 2023 wildfires. Examining the monthly mean profiles from 40°N to 70°N, an increase

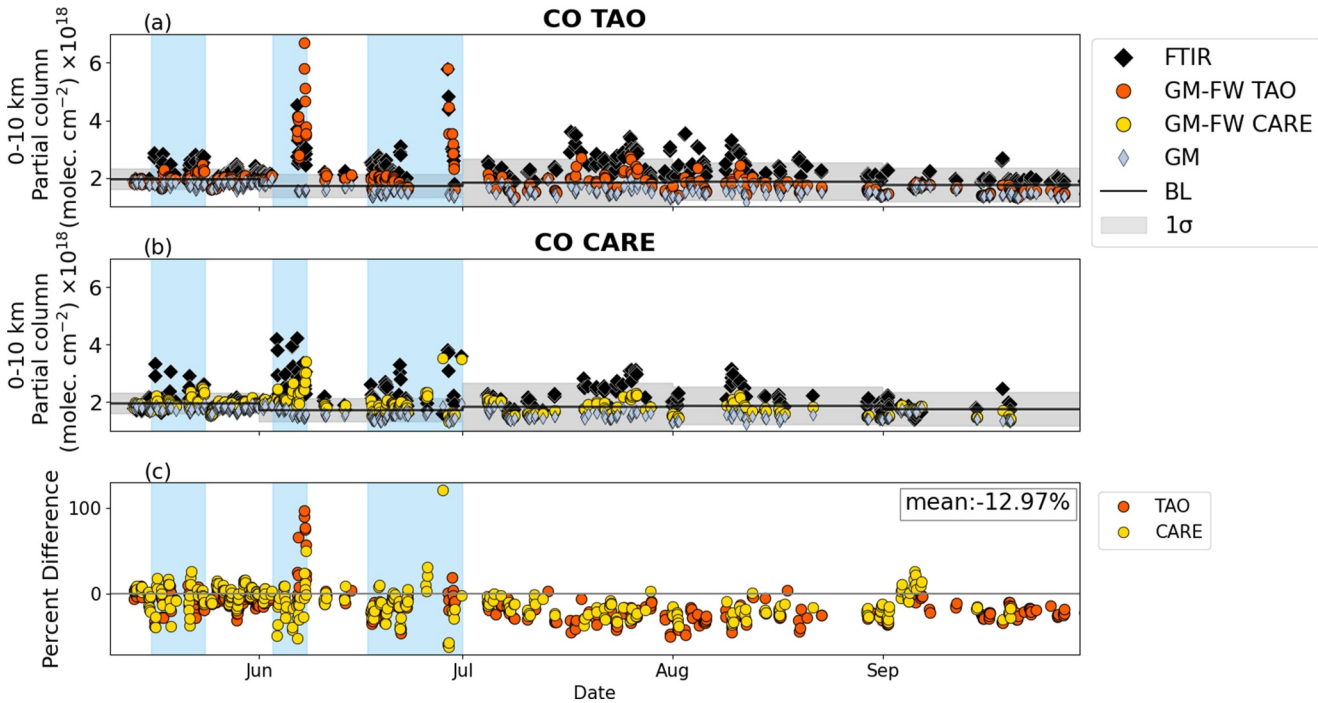

Figure 7. 0–10 km partial column CO at the (a) University of Toronto Atmospheric Observatory (TAO) and (b) Centre for Atmospheric Research Experiments (CARE), from the Fourier transform infrared (FTIR) spectrometers (black diamonds), GEM-MACH (GM) (gray diamonds), and GEM-MACH-FireWork (GM-FW) (orange/yellow points). (c) Percent difference between GM-FW and FTIR for both TAO (orange) and CARE (yellow) (100 × (GM-FW—FTIR)/FTIR). Events 1–3 are marked with blue shading, the black line is the baseline (BL) (monthly mean), and the gray shading is ±1σ of the monthly baseline.

at altitudes between about 8 and 11 km for CO, C_2H_6, CH_3OH, HCN, and HCOOH in 2023, relative to the 2004–2022 mean, was observed. However, the profiles were not significantly enhanced in the stratosphere, indicating that the plumes were transported within the troposphere. This is consistent with the MPLNET and FTIR profiles plotted in Figure 4, in addition to the correlations observed in Figure 6 and the enhancements in the time series (Figures 3 and A1-A6).

4.3. GEM-MACH-FireWork Model-Measurement Comparisons

This section evaluates the GM-FW outputs around Toronto and Egbert with FTIR partial column and OMECP surface measurements, and more broadly across Canada with time-averaged total columns from MOPITT. This allows for an assessment of the location-specific model performance at the surface and through the troposphere, and a broader perspective of long-range transport. GM (without fire emissions) is shown in the column FTIR and surface comparisons (Figures 7–9 and 11) to highlight and quantify the difference caused by the fire emissions, specifically when GM-FW values are above those of GM. Table 2 outlines the mean percent difference and NRMSE spanning May through September, by gas and location for the FTIR and surface comparisons.

4.3.1. Tropospheric Column Comparisons

Figures 7–9 show the time series of the 10 km partial columns of CO, NH_3 and O_3 from the FTIRs and corresponding model simulated column densities (both GM and GM-FW) for TAO (panel a) and CARE (panel b), where the points are time-matched, as described in Section 3.3. Similar to Figure 3, the baseline is indicated with a black line, and ±1σ is represented with gray shading. Panel *c* of Figures 7–9 shows the percent difference between the GM-FW and FTIR partial columns for both locations. As the model values are aligned with the FTIR using information from the retrieval, as outlined in Section 3.3, model results are only applicable when there is a corresponding FTIR measurement. Figure A11 shows the time-matched GM-FW partial columns versus the FTIR partial columns of CO, NH_3, and O_3 with a line representing the linear relationship for each location, and a black line representing a 1:1 ratio. Generally, in the 0–10 km partial column the model underestimates background concentrations of CO, NH_3, and O_3 with the overall percent difference across the May—September period for the

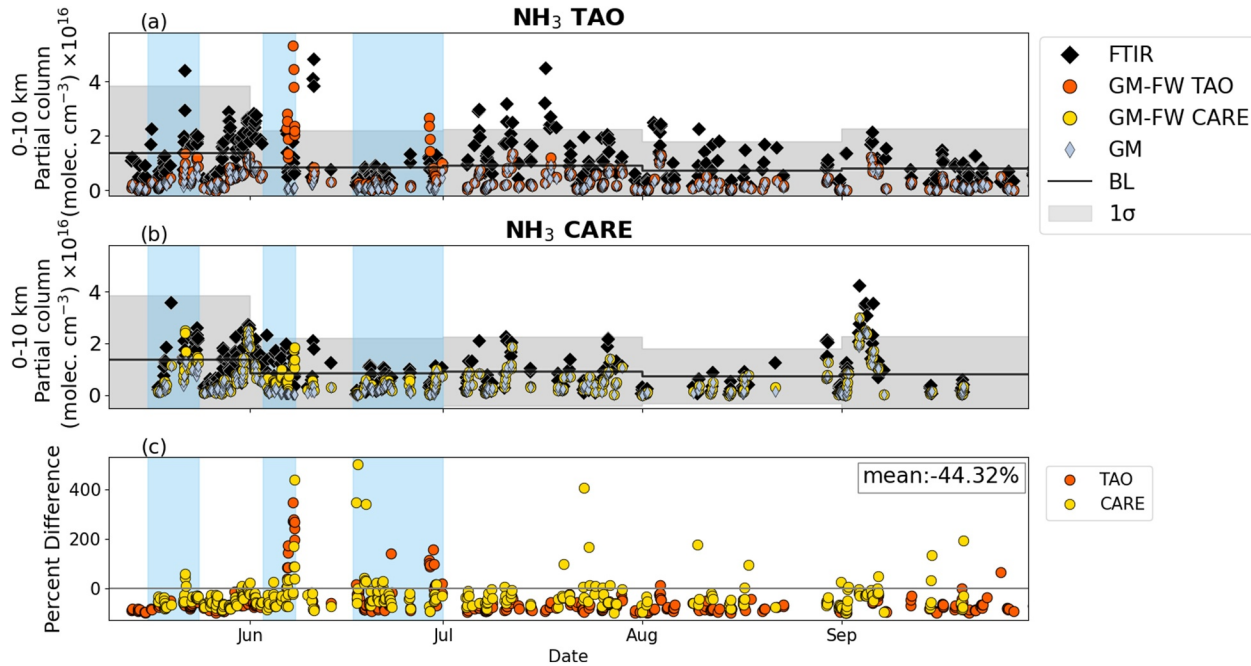

Figure 8. 0–10 km partial column NH_3 at the (a) University of Toronto Atmospheric Observatory (TAO) and (b) Centre for Atmospheric Research Experiments (CARE), from the Fourier transform infrared (FTIR) spectrometers (black diamonds), GEM-MACH (GM) (gray diamonds), and GEM-MACH-FireWork (GM-FW) (orange/yellow points). (c) Percent difference between GM-FW and FTIR for both TAO (orange) and CARE (yellow) (100 × (GM-FW—FTIR)/FTIR). Events 1–3 are marked with blue shading, the black line is the baseline (BL) (monthly mean), and the gray shading is ±1σ of the baseline.

combination of TAO and CARE being −12.97%, and −44.32%, and −21.73% respectively. These negative biases (Table 2) are greater than the FTIR measurement uncertainties (Table 1) and may indicate that the anthropogenic emissions (or subsequent chemistry) of these species is underestimated.

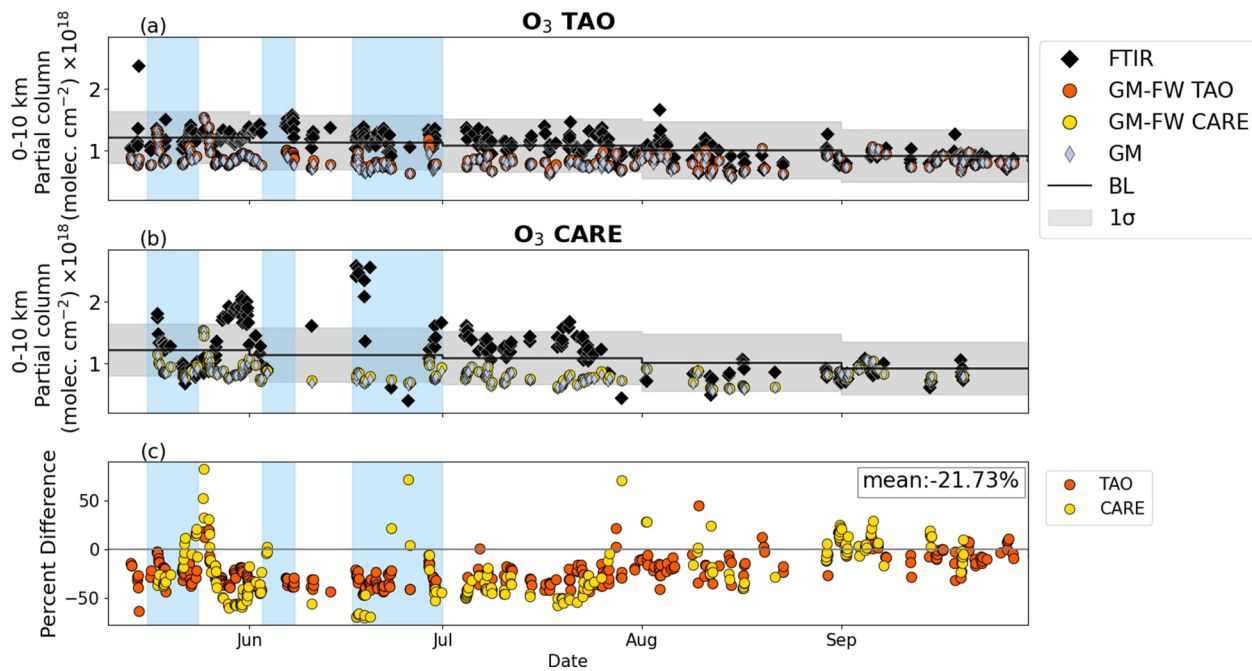

Figure 9. 0–10 km partial column O_3 at the (a) University of Toronto Atmospheric Observatory (TAO) and (b) Centre for Atmospheric Research Experiments (CARE), from the Fourier transform infrared (FTIR) spectrometers (black diamonds), GEM-MACH (GM) (gray diamonds), and GEM-MACH-FireWork (GM-FW) (orange/yellow points). (c) Percent difference between GM-FW and FTIR for both TAO (orange) and CARE (yellow) (100 × (GM-FW—FTIR)/FTIR). Events 1–3 are marked with blue shading, the black line is the baseline (BL) (monthly mean), and the gray shading is ±1σ of the baseline.

As seen in Figure 7c, the GM-FW model underestimated the enhancements in the tropospheric partial columns of CO for Event 1, relative to the FTIR in both locations. Although there are a few points with a positive bias, these do not correspond to the enhanced FTIR measurements. For Event 2, the magnitude of enhancements in GM-FW CO are low in comparison to those measured in the earlier days of the event by the FTIRs, appearing minimally enhanced compared to GM (as seen in Figures 7a and 7b), until toward the end of the event (June 6-7). Throughout Event 2, the CO at CARE is generally underestimated, however the maximum column is overestimated at TAO, showing some instances with larger partial columns than in Event 3. Similar to Event 2, the GM-FW values for Event 3 have minimal increases between GM and GM-FW until later in the event when the maximum enhancements are reached, though these are well represented by GM-FW relative to the FTIRs. The lag between enhancements recorded by the FTIRs and those simulated by GM-FW may indicate that modeled plume transport was slower than reality. The assorted CO enhancements seen in the FTIR time series throughout the rest of the season are also underestimated by GM-FW, with an overall mean difference of −12.97%. Despite some differences between locations during the events, the overall biases and NRMSE for GM-FW relative to the FTIR tropospheric CO partial columns are comparable (−15.37%/1.25 for TAO and −10.26%/1.11 for CARE, respectively).

NH_3 was enhanced above the baseline $+1\sigma$ for Event 1 (Figure 8), though GM-FW simulated enhanced NH_3 for all three events. The NH_3 is better represented at CARE compared to TAO with approximately 25% difference in the mean bias and a NRMSE of 0.82 versus 1.34 (see Table 2). The difference between the rural and urban locations may indicate that a local emission source(s) is underrepresented in the model. Comparing satellite-derived emission ratios to the GM-FW modeled values from the Alberta Horse River fires, Adams et al. (2019) reported that the NH_3/CO ratio was in good agreement (approximately 1.5 times lower in the model). Comparing this finding with the overestimation of NH_3 during the events seen in Figure 8, suggests the model assigns a reasonable NH_3 emission at the source, but has a lifetime that is too long. In addition, background NH_3 may be underestimated by the model due to a lack of the bidirectional flux process (Farquar et al., 1980). The re-emission of deposited NH_3 was added in a research version of GM and shown to reduce its negative bias in background conditions (Whaley et al., 2018), but is not included in the operational version of the model used in this work.

O_3 enhancements were measured during Events 1 and 3 at CARE, but not for any events at TAO. GM-FW simulated only very small increases in O_3 during Event 3 at TAO. The overall O_3 percent difference for both TAO and CARE are on the order of −21%, while the NRMSE is somewhat better for CARE at 1.34 versus 1.64 at TAO.

The vertical profiles retrieved with the FTIR were compared with those from GM-FW, Figures 10a–10c shows the mean VMR profile for each event, and the monthly mean baseline profiles for May and June. To assess the altitude and magnitude of enhancements, Figures 10e and 10f shows the mean "percent enhancement" profiles for GM-FW and the TAO FTIR over each event (similar to Figures 4a–4c). The mean FTIR profiles are made using all of the available measurements during each of the three events, while the percent enhancement is the percent difference between the event-averaged profile and the relevant monthly mean baseline profile. The mean profile for GM-FW uses all of the days during each of the three events, limited to 7 a.m. to 7 p.m. to reflect the daytime constraint of the FTIRs, while the enhancement profile is defined relative to the corresponding mean GM profile. These differences aim to represent the percent contribution from the wildfire emissions at the time of the events, relative to the background VMRs.

GM-FW and the FTIR both show the CO maximum in the lowest layers near the surface for Events 2 and 3. But for Event 1, the model shows a vertical profile where CO was at a maximum around 4 km aloft (Figure 10a). The FTIR profile does not quite match that, however, its vertical resolution is lower, and it is influenced by the a priori profile shape. The CO attributed to the smoke plumes (Figure 10d) is generally overestimated at their peaks relative to the FTIR, but this could be due to the FTIR's lower vertical resolution. The GM-FW CO VMR for event 2 at TAO is overestimated by about 50% in the lowest 3 km, which is consistent with the results seen in Figure 7.

The smaller NH_3 and O_3 enhancements in the FTIR measurements during the events, as seen in Figures 6, 8, and 9, is reflected by overlap of the FTIR event profiles with the May and June monthly means (gray lines in Figures 10b and 10c), and consequently the FTIR profiles show less distinct patterns between events. It is clear from Figure 10e that the GM-FW NH_3 is significantly overestimated in all three events relative to the GM, at altitudes ranging from ∼1 to 3 km for Event 3, to 3.5–5.5 km for Events 1 and 2. This may be less obvious in the time series plots as some of the extreme NH_3 outliers by GM-FW that are creating the high bias may be missed by gaps in the FTIR measurements and/or reduced by the smoothing routine; nonetheless, there are still instances where the GM-FW minus FTIR difference is over 400% (Figure 8c). O_3 enhancements in GM-FW are primarily

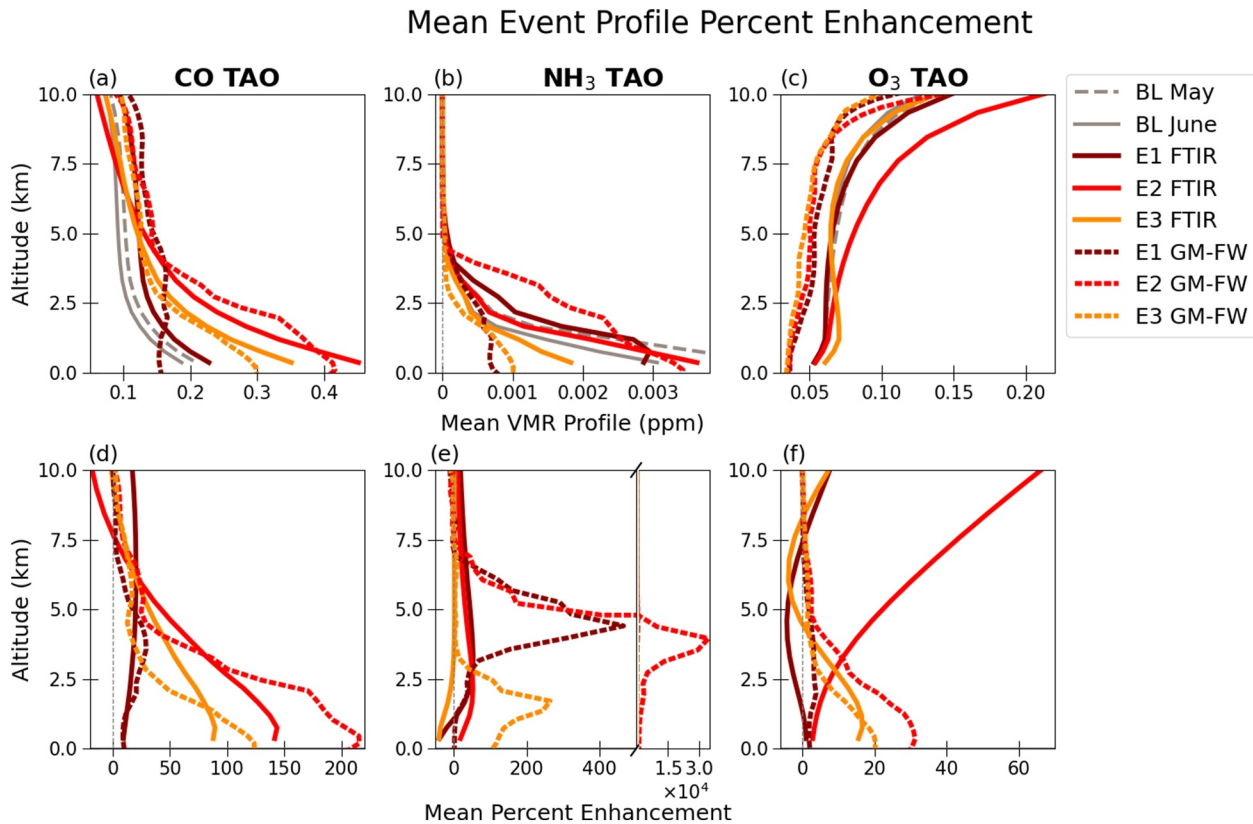

Figure 10. (a–c) The mean volume mixing ratio (VMR) profile by event (E) from the University of Toronto Atmospheric Observatory (TAO) Fourier transform infrared (FTIR) spectrometer (solid lines) and GEM-MACH-FireWork (GM-FW) (dashed lines), and the monthly mean May and June baseline (BL) profiles (gray). (d–f) The mean percent enhancement profiles for each event; solid lines are 100 × (TAO FTIR event-averaged profile—the relevant monthly mean baseline profile) and dashed lines are 100 × (GM-FW event-averaged profile—GM event-averaged profile).

seen in the lower 2.5 km for Events 2 and 3, while the FTIR enhancement profiles oscillate around the monthly mean baselines. The variability in O_3 enhancements may be a result of competing processes; O_3 enhancements from fire can occur from the emitted VOCs interacting with urban NO_x pollution, however reduced photolysis in smoke plumes may cause a reduction in O_3.

Table 2
Mean Percent Difference and Normalized Root Mean Square Error for the Comparisons of GM-FW to Measurements of Tropospheric Columns and the Surface Concentrations for CO, NH_3, O_3 and $PM_{2.5}$ From May-September 2023

		Tropospheric column		Surface	
		TAO	CARE	Toronto	Barrie
CO	*Mean % Difference*	−15.37	−10.26	28.98	/
	NRMSE	1.25	1.11	1.73	/
NH_3	*Mean % Difference*	−55.92	−30.49	/	/
	NRMSE	1.34	0.82	/	/
O_3	*Mean % Difference*	−21.61	−21.95	−24.07	−5.43
	NRMSE	1.64	1.34	1.37	0.85
$PM_{2.5}$	*Mean % Difference*	/	/	52.24	−52.02
	NRMSE	/	/	1.34	0.87

4.3.2. Surface Comparisons

Figure 11 shows the GM (gray diamonds) and GM-FW (Toronto in orange and Barrie in yellow) daily surface means compared to the OMECP daily mean surface concentrations for CO, O_3 and $PM_{2.5}$ (black diamonds). The model results are extracted at the closest location to each OMECP station. The bottom row (panels f–h) shows the percent differences between the daily surface GM-FW and surface measurement, with the mean percent difference representative of all the points on each panel. Figure A12 shows the comparison of daily mean GM-FW versus the OMECP for CO, O_3 and $PM_{2.5}$, and Table 2 shows the mean percent difference and NRMSE by location. Using the summer mean values from Table A2 and the instrument detection limits from Section 2.2, the approximate percent uncertainty is 10% for surface CO, <2% for surface O_3, and approximately 5% for surface $PM_{2.5}$ at Toronto, and <1% for surface $PM_{2.5}$ at Barrie. Comparing these to the mean percent differences in Table 2, the model bias outweighs the uncertainty in each case.

The OMECP surface CO shows a few enhancements throughout the summer (see Figure A10c). As seen in Figure 11a, both GM and GM-FW often

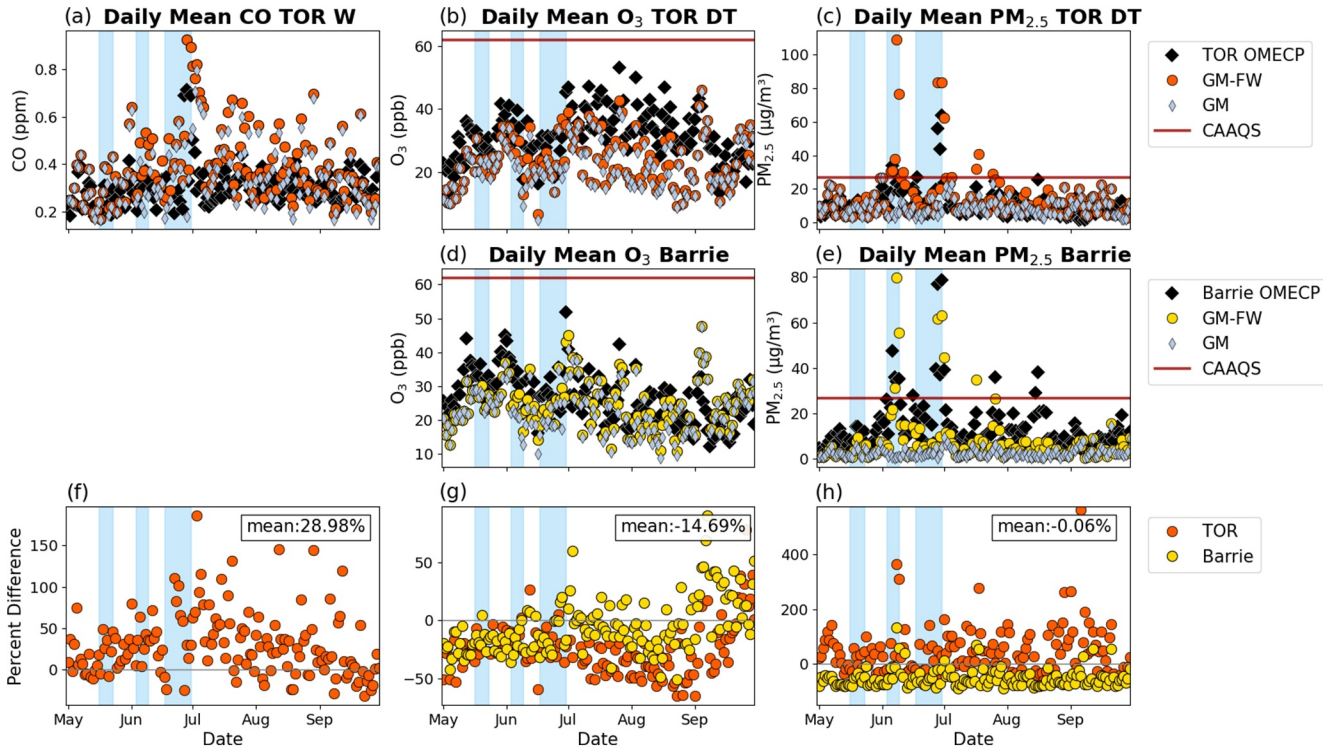

Figure 11. Daily mean surface values from the Ontario Ministry of Environment, Conservation and Parks (OMECP), GEM-MACH (GM), and GEM-MACH-FireWork (GM-FW) for (a) CO (Toronto West) (b), (d) O_3 (Toronto Downtown and Barrie) and (c), (e) $PM_{2.5}$ (Toronto Downtown and Barrie), with the Canadian Ambient Air Quality Standard (CAAQS) indicated by the red line. (f)–(h) The percent difference between GM-FW and OMECP (100 × (GM-FW—OMECP)/OMECP). The mean differences in panels f–h is for all the points combined.

overestimate the surface CO. GM-FW shows more surface enhancements (in frequency and value) than the OMECP measurements. Furthermore, there are points from GM that are enhanced relative to an average day, implying a direct anthropogenic source, even at times when the CO is likely related to fire emissions (e.g., following Event 3), suggesting that the fire emissions only contributed a small amount to the enhanced CO at that time. Both observations and GM-FW showed greater fire enhancements in the CO column compared to the surface, indicating a roughly accurate modeled vertical distribution of CO from the fire emissions. However, the positive surface bias, compared to the negative tropospheric column bias, may indicate that the model overestimates CO at the surface and poorly characterizes the vertical distribution of background CO.

Surface O_3 is generally underestimated by GM and has only a few points from GM-FW that are enhanced due to fire emissions during Events 2 and 3. The mean percent difference for both tropospheric column comparisons and Toronto surface comparisons are all similar (−21% to −24%). The Barrie station has a smaller bias of −5.43% and NRMSE of 0.85, however this may be impacted by the upward trend seen in September (see Table 2 and Figure 11g).

GM-FW $PM_{2.5}$ shows a mean overestimation of 52% at Toronto, and a mean underprediction of 52% in Barrie, which results in a near 0 mean difference when the results from the two locations are combined (see Table 2 and Figure 11h). The GM points in Figure 11 also show this difference, which suggests there is an overestimation of urban emissions, and underrepresentation of rural emissions within the model. However, the timing in $PM_{2.5}$ enhancements from smoke is captured within the model, though with inconsistent magnitudes. The $PM_{2.5}$ biases may be influenced by the above mentioned differences in NH_3 (Figure A12c and Table 2).

4.3.3. Satellite Comparisons

Figure 12 shows the GM-FW and MOPITT mean total column CO over Canada for each event period, where the location of TAO and CARE is marked with a cyan circle. Although the model has a higher spatial resolution than the satellite (22 km × 22 km for MOPITT vs. 10 km × 10 km for GM-FW) potentially leading to larger peak

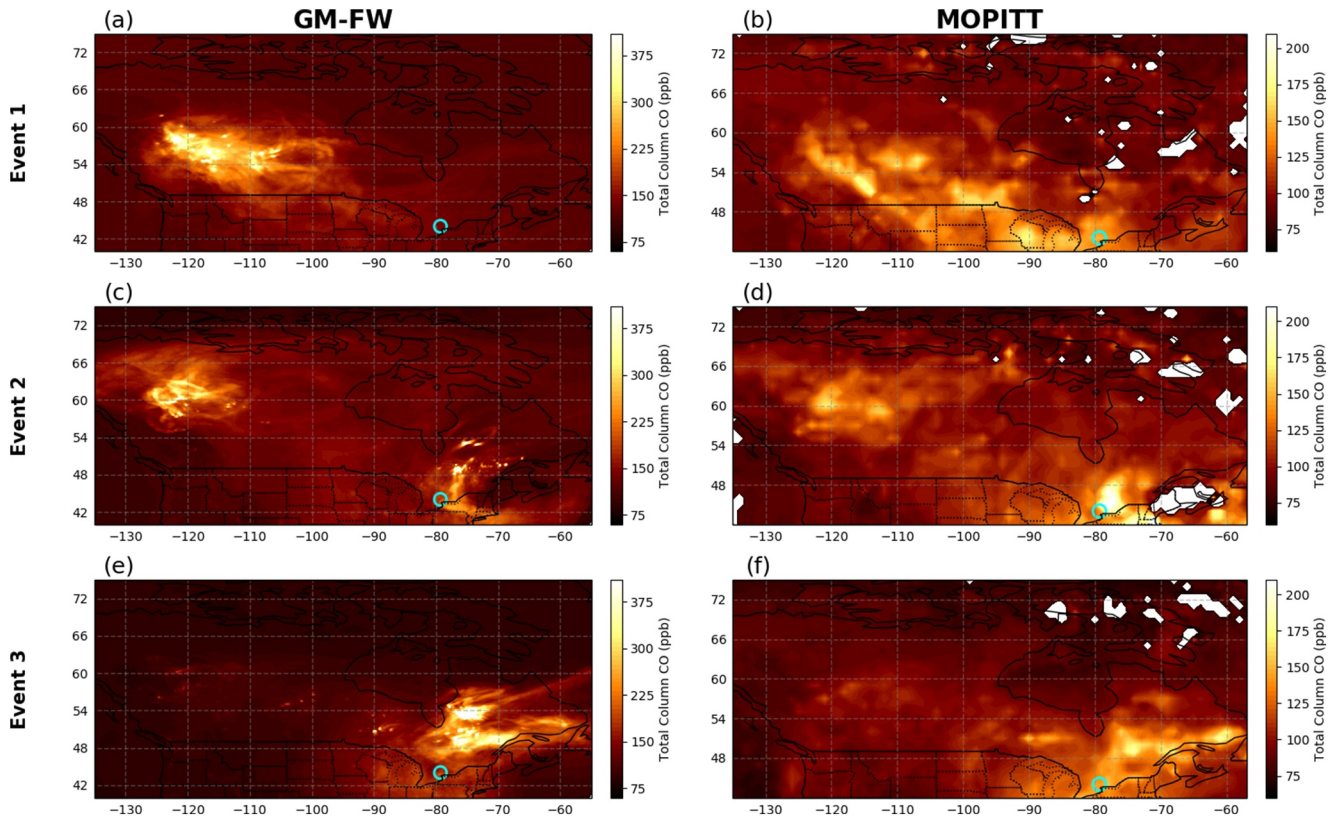

Figure 12. Mean total column CO (ppb) during each of the three events (May 16-23, June 3-9 and June 17-30, 2023), from GEM-MACH-FireWork (GM-FW) (a, c, e) and Measurements of Pollution in the Troposphere (MOPITT). (b, d, f). The general area of the University of Toronto Atmospheric Observatory and the Centre for Atmospheric Research Experiments is marked with a cyan circle.

values, overall, the regions with notable enhancements are comparable. This indicates that the model effectively represents the long-range transport of CO during the smoke events, which indirectly indicates that the fire plume height of the emissions is probably accurate.

Figure 13 shows the same information as Figure 12, but zoomed into Southern Ontario, including Toronto and Egbert. Panels a and b show that for Event 1, when both TAO and CARE CO were underestimated by the model (as seen in Figure 7), the model versus MOPITT results are spatially consistent. This implies that the model's event-averaged plume was in the correct location, however, overall, the model is underestimating the mean CO over Event 1. Panel a and b in Figure 13 may indicate that this is related to resolution, where MOPITT measurements are coarser. For Event 2, Figure 7 showed that the model overestimated CO at TAO, but underestimated CO at CARE. From Figure 13c/d, it looks like the event-averaged plume was not actually over either site during Event 2—according to MOPITT, it was to the east of both sites—but GM-FW located it further to the south, thus causing the overestimation at TAO, but not at CARE. Finally, for Event 3, Figure 7 implied that the model CO matched well for TAO, but was a little underestimated for CARE. Figure 13e/f is again consistent with Figure 7, and shows that this underestimation was because the area of reduced CO in GM-FW was closer to CARE than to TAO, while that reduced CO area was located even further west in the MOPITT measurements.

5. Conclusions

The unprecedented intense wildfire season of 2023 in Canada burned approximately 4% of Canada's forested area, resulting in widespread evacuations and air quality warnings (Jain et al., 2024). Above-average heat anomalies and prolonged dry conditions contributed to what is the largest burn season in Canadian history. Understanding how long-range transport of wildfire plumes affects atmospheric composition and air quality is crucial, particularly in a changing climate. Despite the distance from the fires, Southern Ontario experienced several smoke plume events, some of which led to degraded air quality (see summary Table A2 for comparison of CO, O_3 and

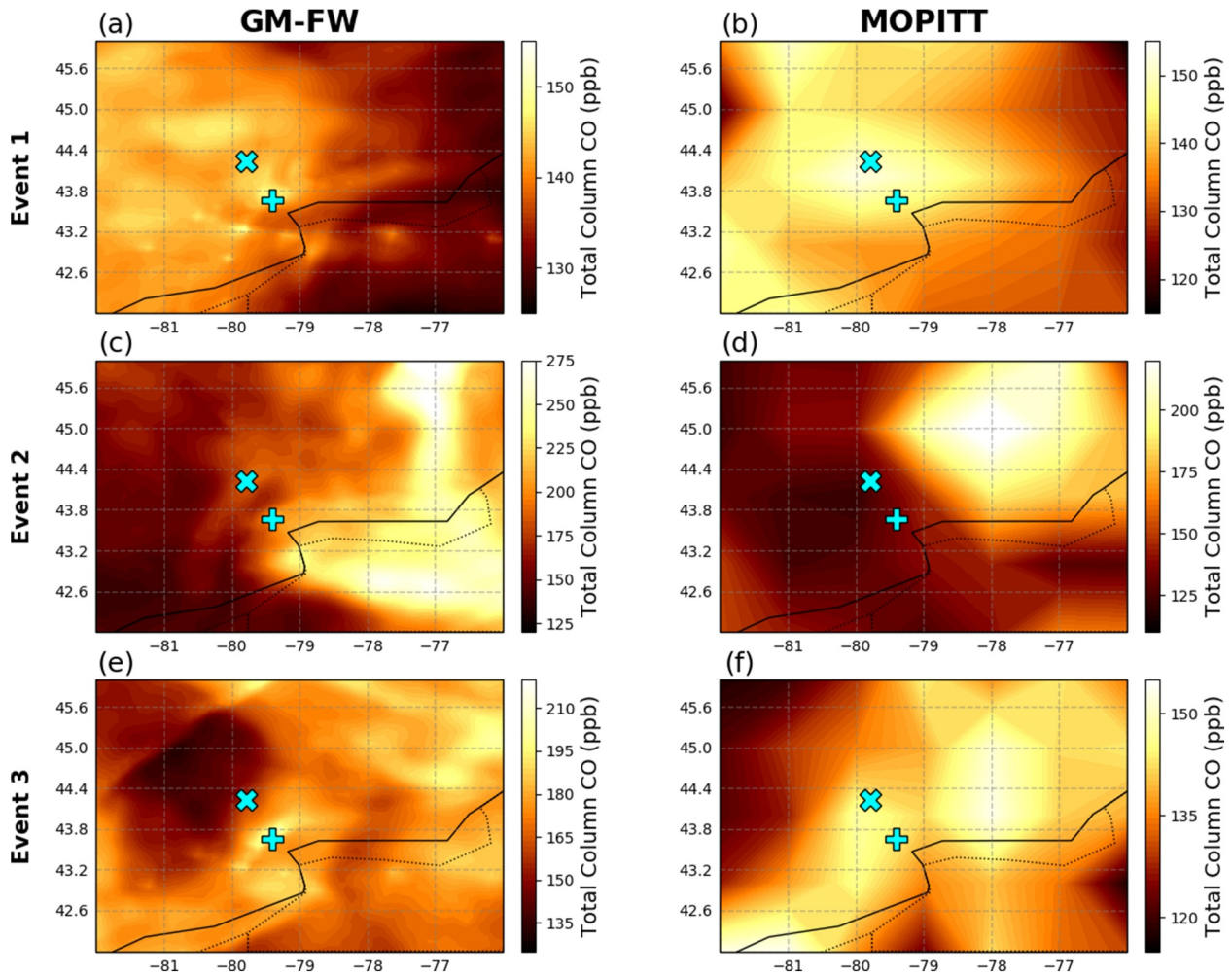

Figure 13. Same as Figure 12, zoomed into the area of Southern Ontario (Centre for Atmospheric Research Experiments marked with the cyan 'X', University of Toronto Atmospheric Observatory marked with the cyan '+'). Note that the scales have changed from Figure 12 and differ between panels to better illustrate the dynamic range.

$PM_{2.5}$ with 5 year mean). The trace gases CO, C_2H_6, CH_3OH, HCN, and HCOOH were found to be elevated in the troposphere in relation to long-range transport from fires in Western Canada and Quebec. Profile analysis using the relative enhancement of CO measured by the TAO FTIR and the NRB from a MiniMPL shows that the smoke layer in Toronto was at an altitude of approximately 5 km for early season events and reached altitudes below 1 km at the peak of severity. Back-trajectories indicate that enhancements came from both Western Canada and Quebec, with similar patterns of long-range transport for the areas of Toronto and Egbert. Three events were examined in detail, where Event 1 (May 16-23) primarily came from fires in the Prairie region with smoke residing at about 5 km, and having little impact on air quality. Event 2 (June 3–9) shows air coming from Quebec in both the 1 and 5 km layers, resulting in moderate air quality degradation. Event 3 (June 17-30) shows 1 km air coming from Quebec and 5 km air traveling from the west, resulting in the most significant air quality event for the Toronto region, during the summer of 2023.

The comparisons presented in this paper provide information that can be used to improve the GM-FW model, which ultimately supports operational air quality monitoring in Canada. When compared to the tropospheric column measurements of CO, NH_3 and O_3, GM-FW has an overall negative bias, indicating that anthropogenic emissions may be underestimated. During the smoke events examined, GM-FW shows instances of both over-estimating and underestimating the magnitude of the tropospheric column. This study provides a novel vertical profile comparison between GM-FW and CO, NH_3 and O_3 with ground-based FTIR and satellite instruments, which showed that GM-FW simulated the peak altitudes well, confirmed on large scales with MOPITT data,

though small differences in high-resolution downwind plume locations can impact site-specific results. NH_3 was highly overestimated during fire events, indicating that the NH_3 lifetime is likely too high, and chemical loss/conversion needs to be improved. The model was unable to capture the O_3 profile variability. When compared to OMECP surface values, GM-FW has a high bias for CO and a low bias for O_3, with a high bias for $PM_{2.5}$ in the urban area of Toronto and a low bias in the more rural area of Barrie. The biases for both surface and tropospheric comparisons were greater than the respective measurement uncertainties. Compared with MOPITT total column satellite measurements, GM-FW effectively captures the distribution of CO during smoke events, the small differences shown in the location of the plumes help explain the FTIR-model comparison results. Overall, the model-measurement comparisons show that the GEM-MACH FireWork model is able to represent tropospheric, ground-level, and wide-spread enhancements from wildfire emissions, although the magnitude of these enhancements has room for improvement.

Uncertainties in several parameters, such as emission estimates, plume chemistry, and plume dynamics, are still present and impact modeling capabilities. This evaluation of the operational air quality model used for the AQHI and air quality alerts in Canada presented in this study offers valuable insights for modelers to identify areas of improvement, specifically addressing extreme events, long-range transport, and altitude-dependent enhancement distribution. Further assessment of the sensitivity of the model simulations to variations in emissions and atmospheric lifetimes can help resolve inconsistencies between source and downwind atmospheric composition. Future research could expand on this study by incorporating more years of data and conducting a model sensitivity analysis to assess specific shortcomings in the model.

Appendix A

See Figure A1, Figure A2, Figure A3, Figure A4, Figure A5, Figure A6, Figure A7, Figure A8, Figure A9, Figure A10, Figure A11, and Figure A12. See Table A1, Table A2, and Table A3.

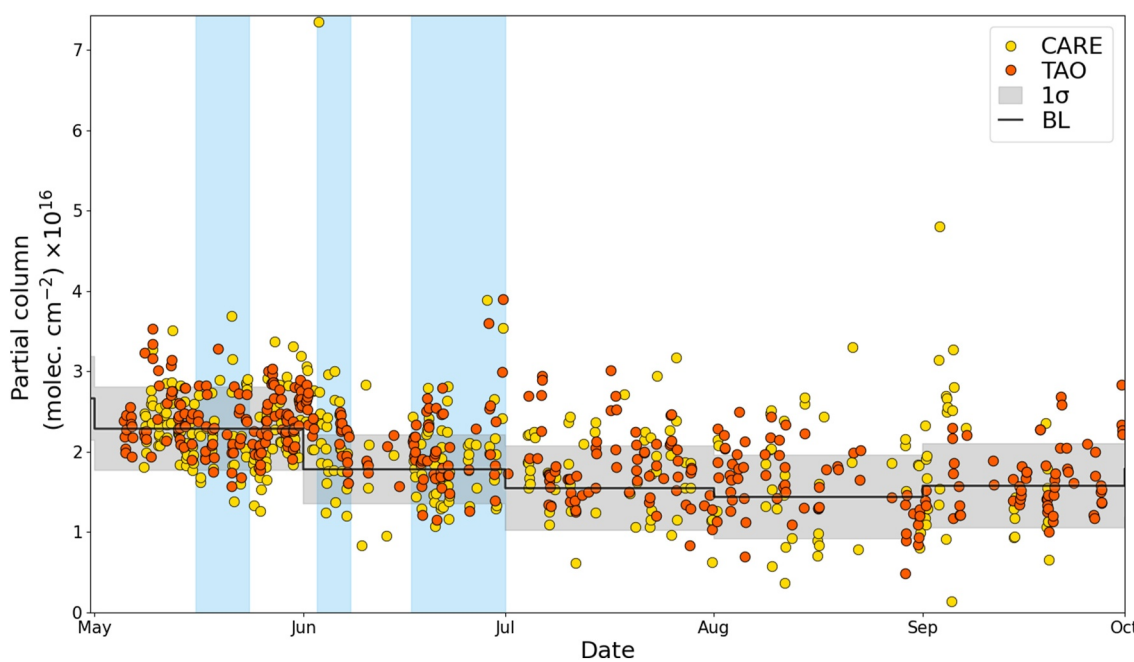

Figure A1. 0–10 km partial column C_2H_6 from the University of Toronto Atmospheric Observatory (TAO) (orange) and the Centre for Atmospheric Research Experiments (CARE) (yellow) for 2023 with the TAO baseline (BL) (black line) ±1σ (gray shaded), and the time of the events marked with a blue shading.

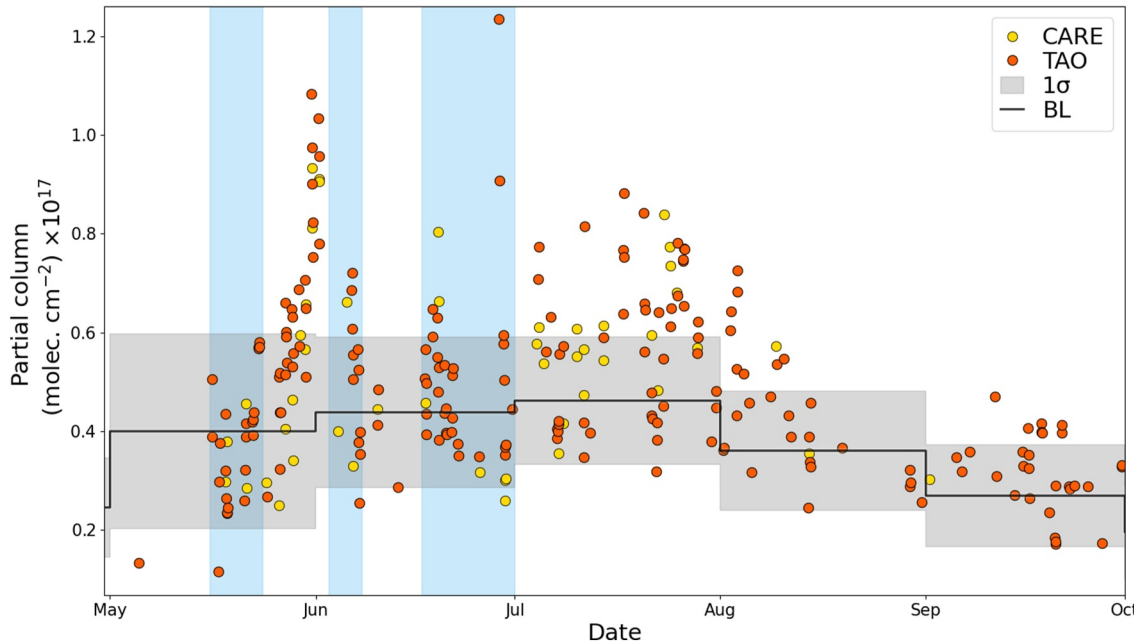

Figure A2. Same as Figure A1 for CH_3OH.

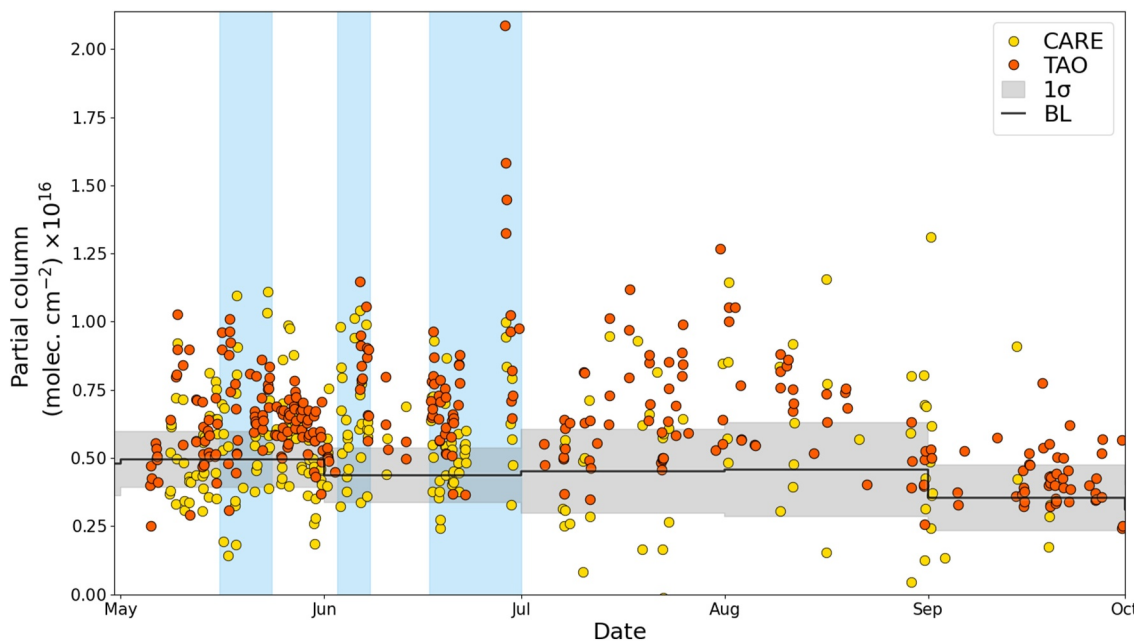

Figure A3. Same as Figure A1 for HCN.

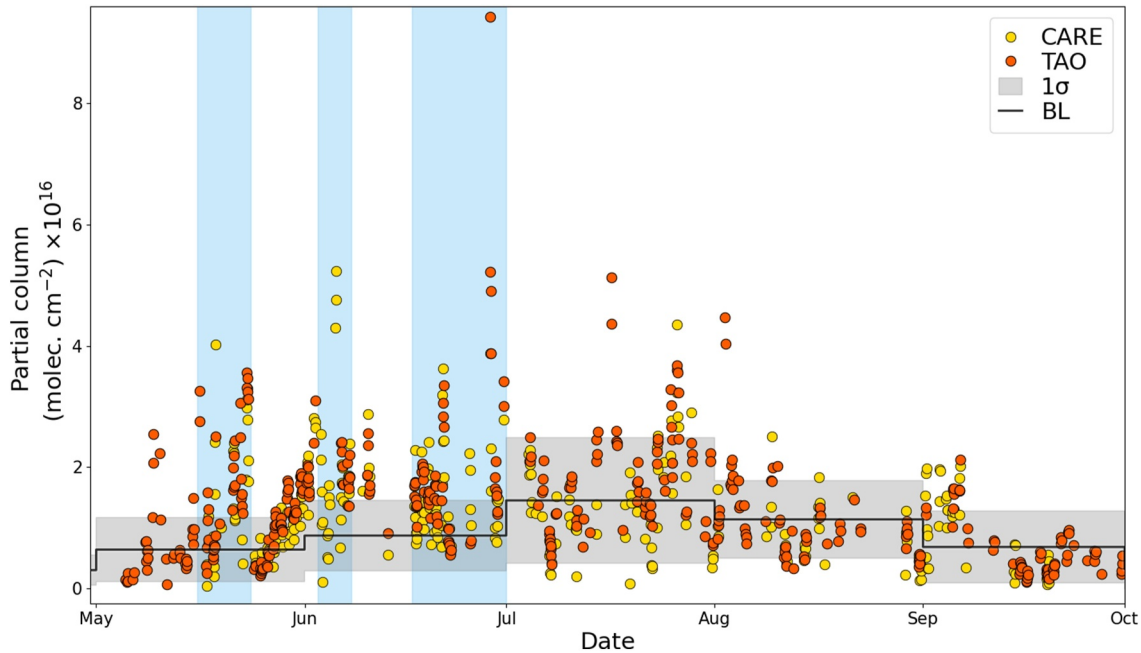

Figure A4. Same as Figure A1 for HCOOH.

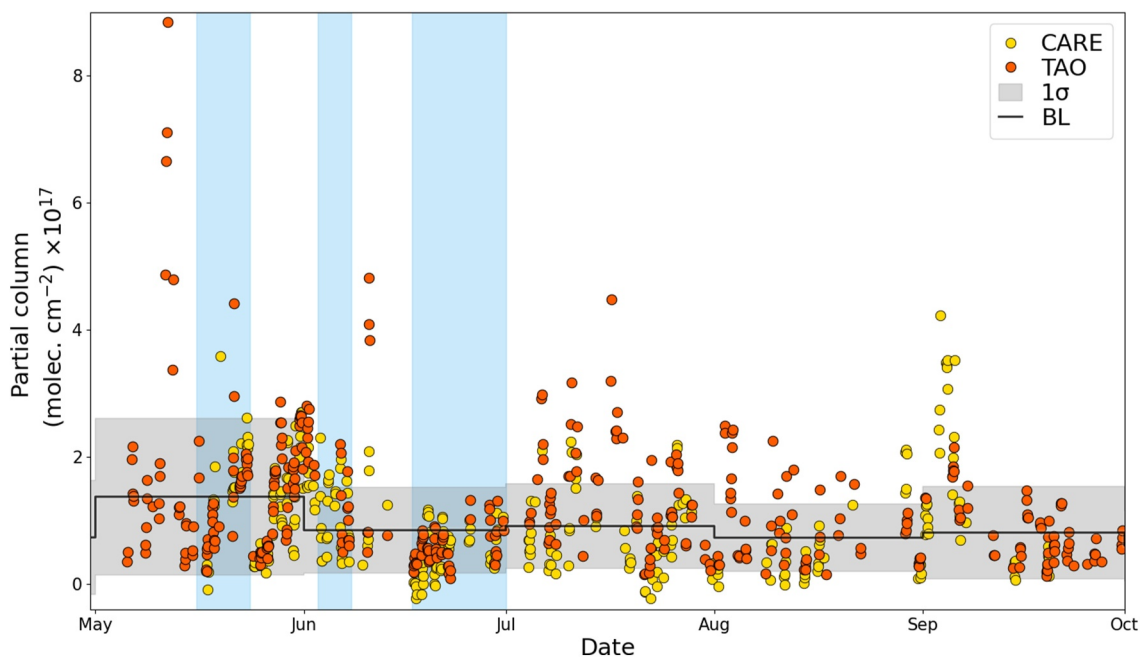

Figure A5. Same as Figure A1 for NH_3.

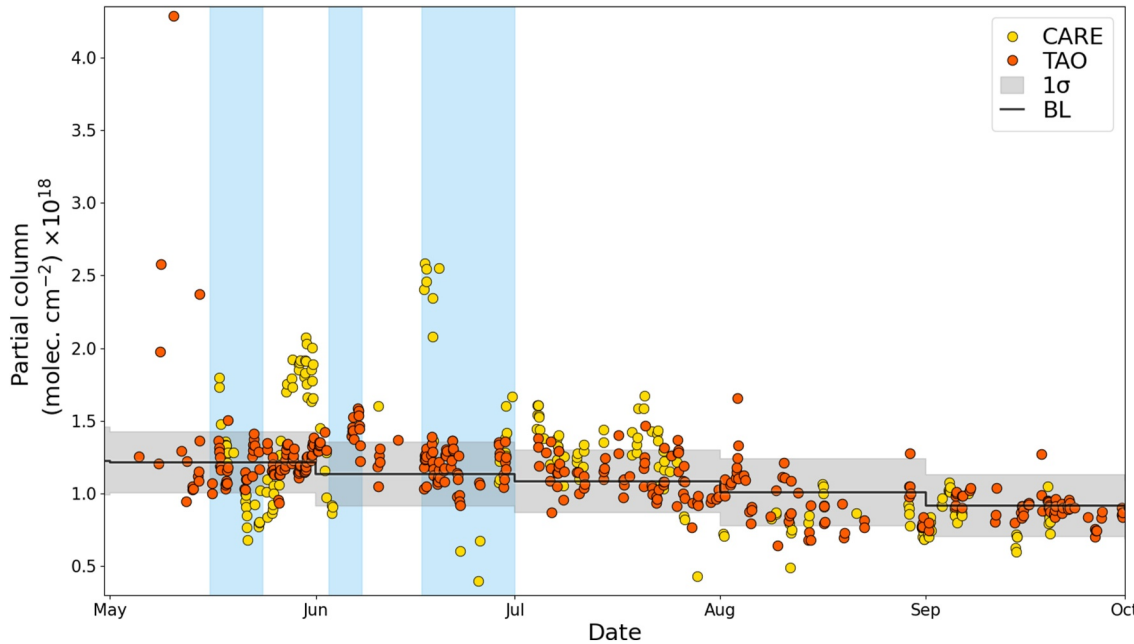

Figure A6. Same as Figure A1 for O_3.

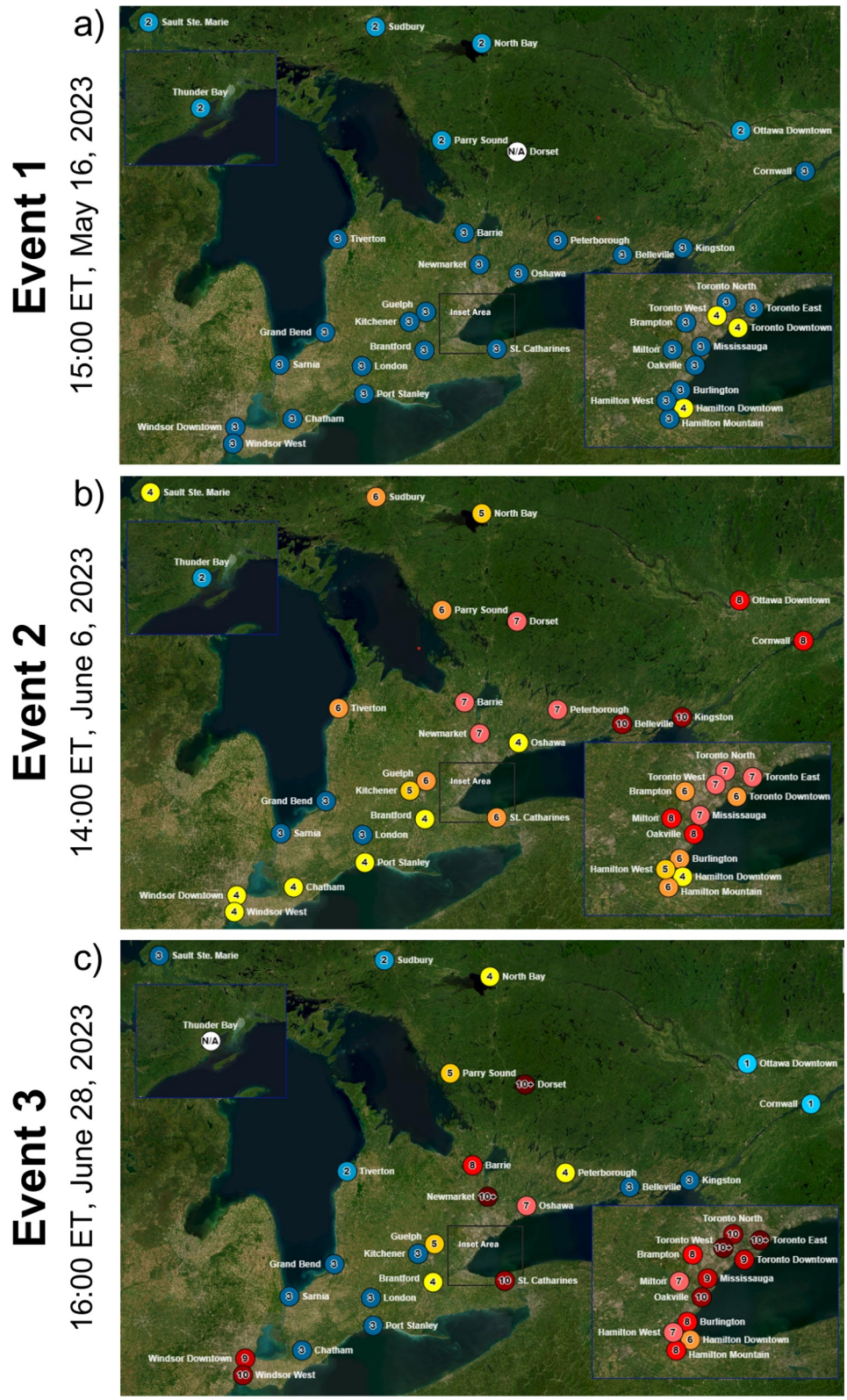

Figure A7. Ontario Ministry of Environment, Conservation and Parks (OMECP) Air Quality Health Index readings for all Ontario stations, corresponding to the time of the Hybrid Single-Particle Lagrangian Integrated Trajectory (HYSPLIT) back-trajectory release (OMECP, 2024) for each of the three events. The number and colour refer to the risk level, 1–3 is low (blue), 4–6 is moderate (yellow/orange), 7–10 is high (pink/red) and 10+ is very high (maroon).

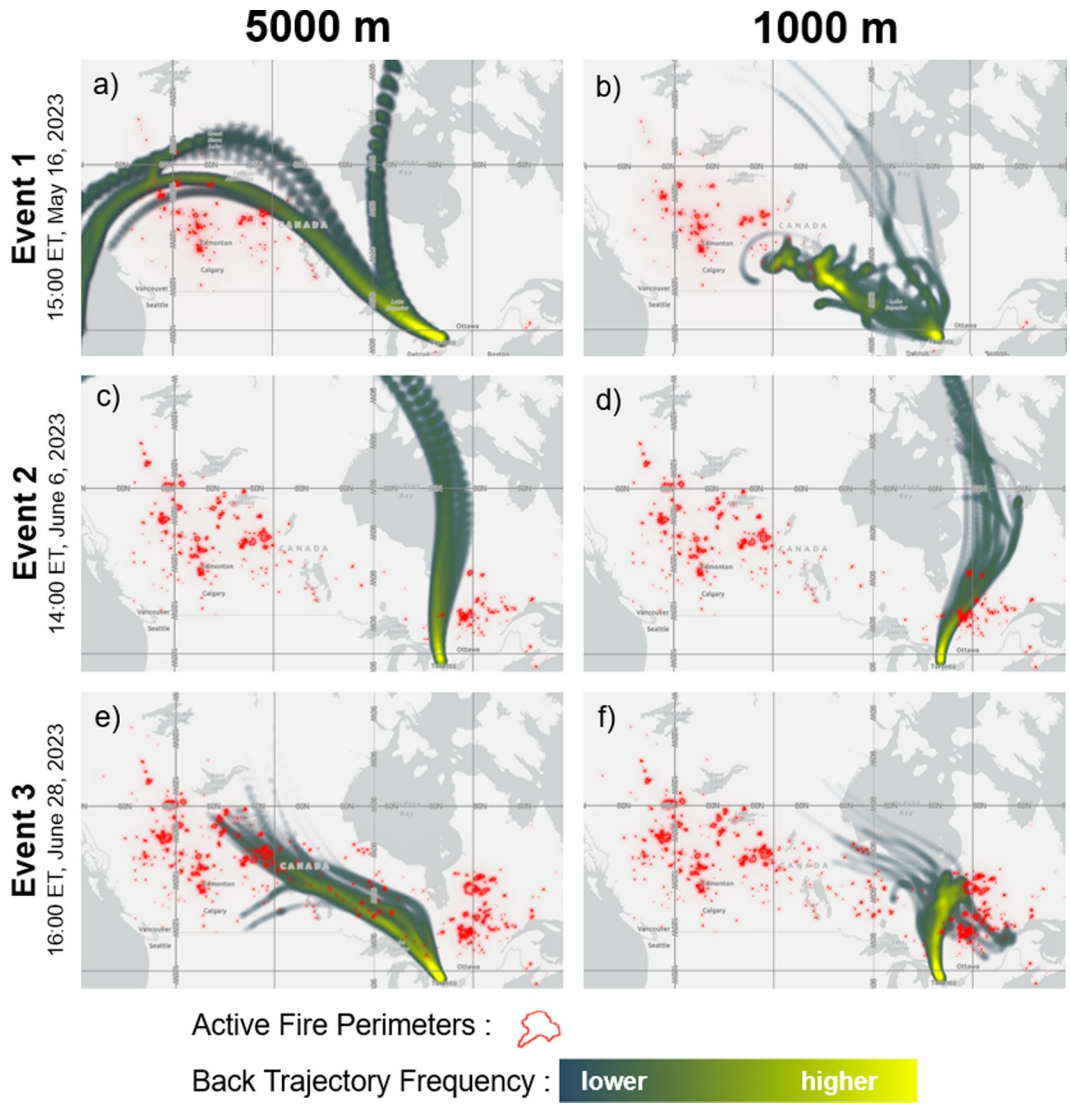

Figure A8. Hybrid Single-Particle Lagrangian Integrated Trajectory (HYSPLIT) 72 hr ensemble back-trajectories, initiated from the Centre for Atmospheric Research Experiments (CARE) at the times listed, from 5,000 m (a, c, e) and 1,000 m (b, d, f). Red polygons represent the active fires at the time (CWFIS, 2024; Esri, 2020).

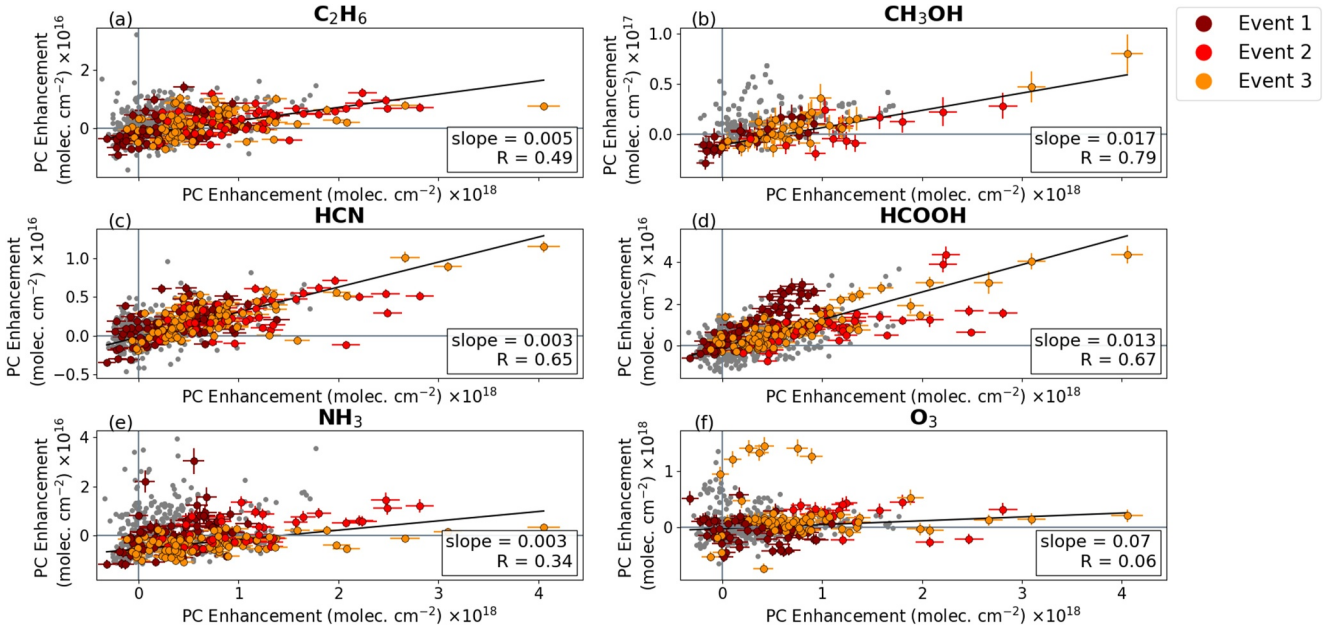

Figure A9. 0–10 km partial column enhancement of biomass-burning-related species versus CO (measured within ±3 hr) for the University of Toronto Atmospheric Observatory (TAO) and the Centre for Atmospheric Research Experiments (CARE) Fourier transform infrared spectrometers from May - September 2023 (gray), with events marked by color. Error-weighted slopes are shown for the combined TAO and CARE datasets with all events.

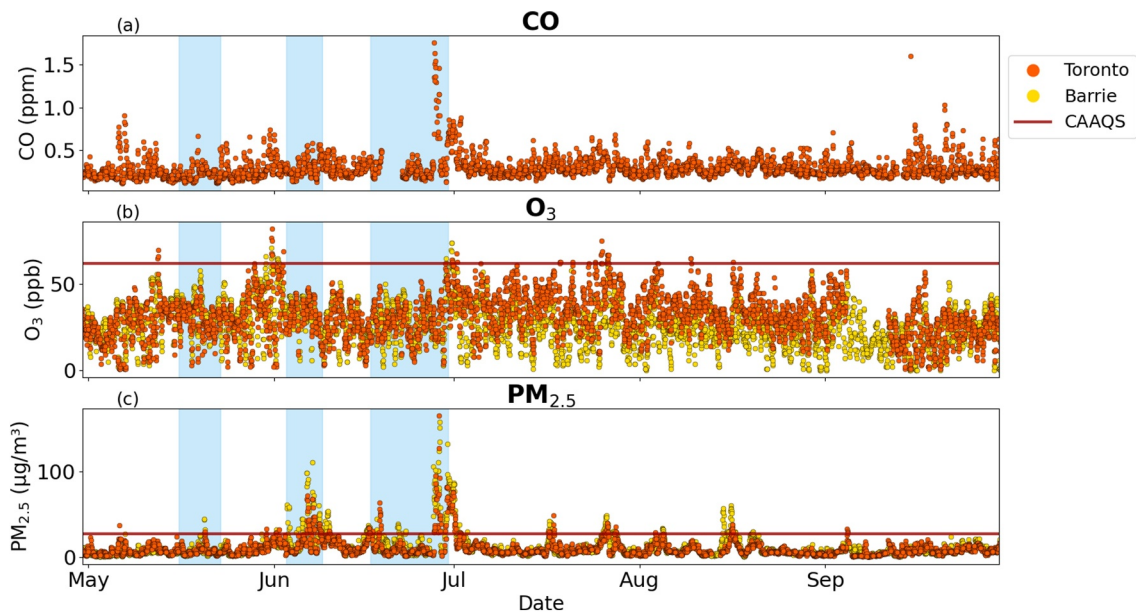

Figure A10. Ontario Ministry of Environment, Conservation and Parks surface CO, O_3, and $PM_{2.5}$ air quality readings for Toronto Downtown/West (orange) and Barrie (yellow), with the Canadian Ambient Air Quality Standard (CAAQS) marked in red.

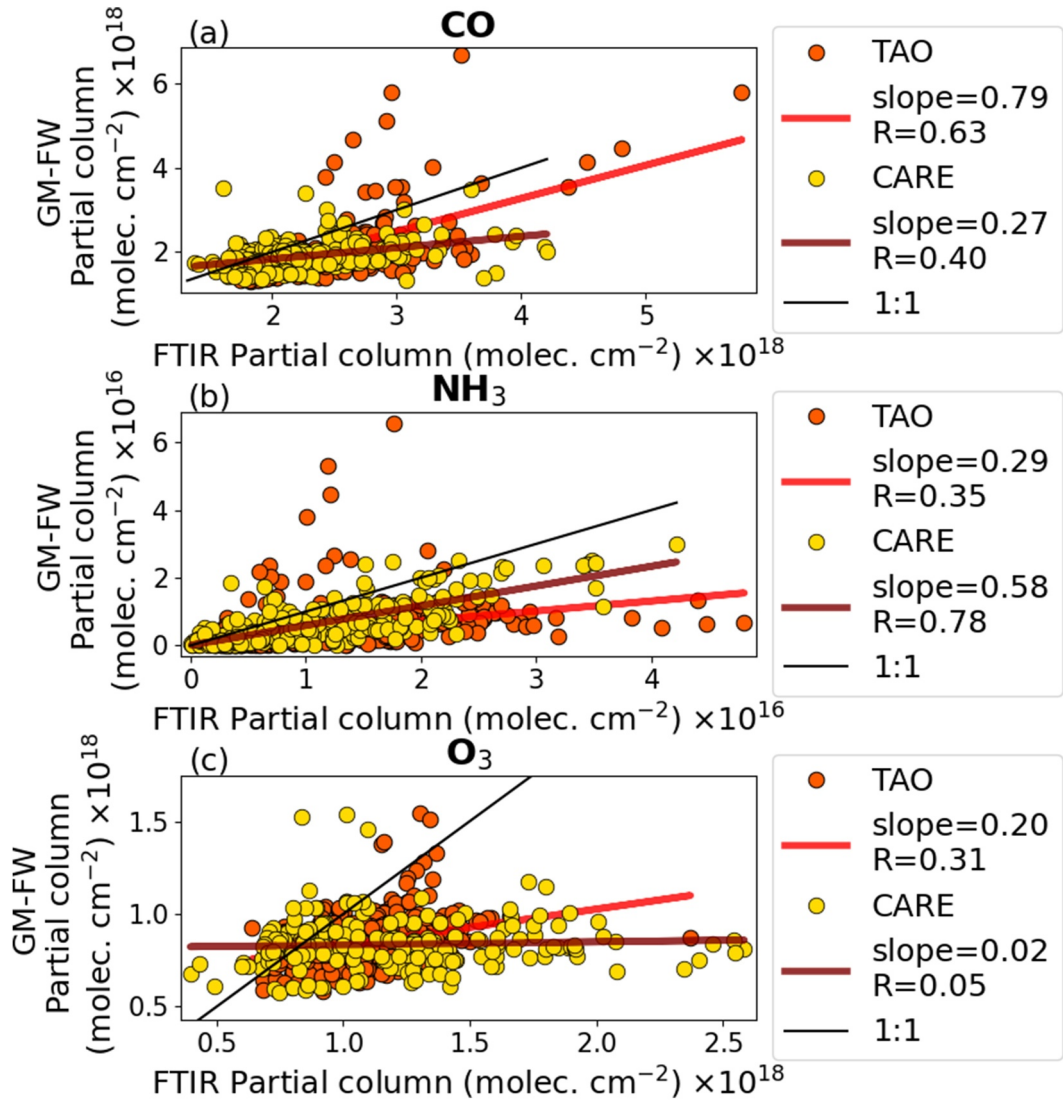

Figure A11. (a) CO, (b) NH_3, and (c) O_3 0–10 km partial columns from GEM-MACH-FireWork (GM-FW) versus Fourier transform infrared (FTIR) spectrometers at the University of Toronto Atmospheric Observatory (orange) and the Centre for Atmospheric Research Experiments (CARE) (yellow), with a linear regression applied. The slope and R of each fit is given in the legend and the black line represents 1:1.

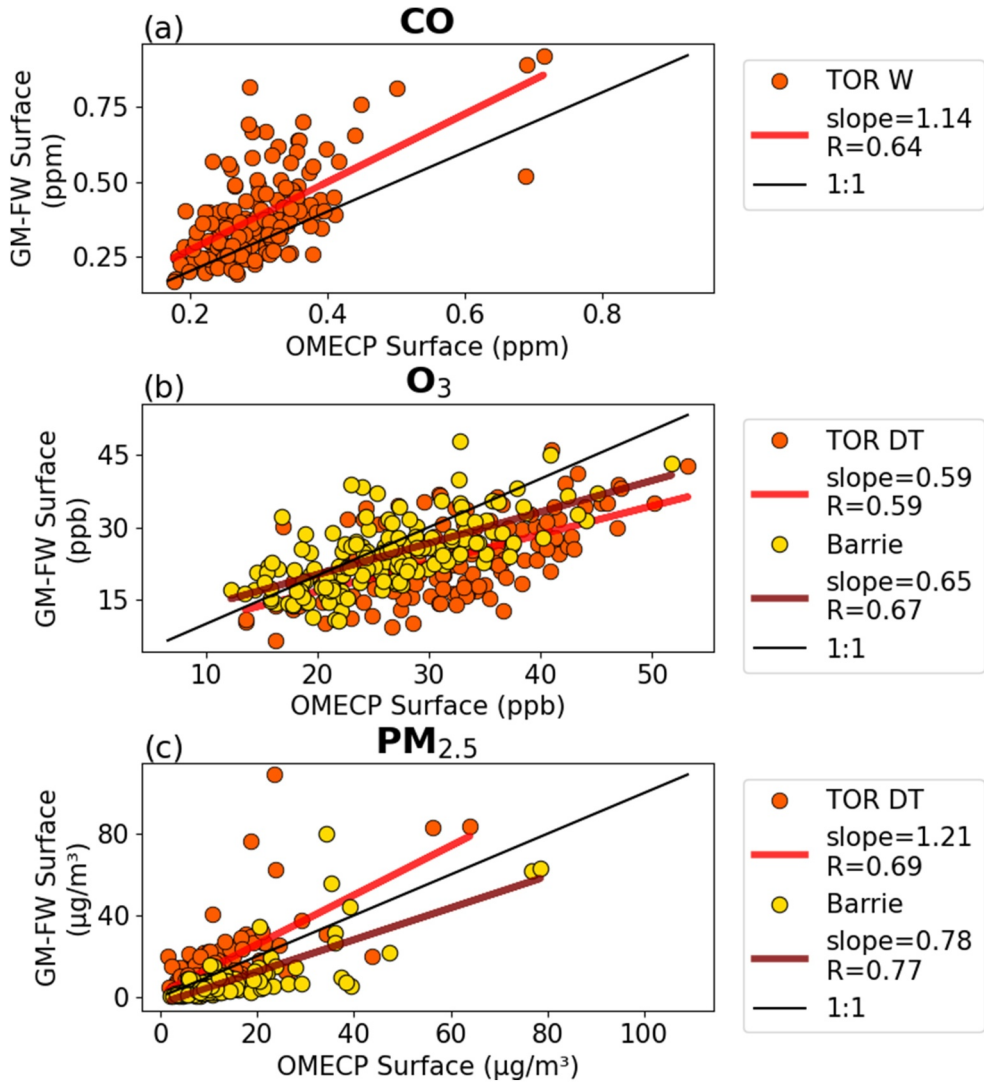

Figure A12. (a) CO, (b) O_3 and (c) $PM_{2.5}$ daily mean surface measurements from GEM-MACH-FireWork (GM-FW) versus Ontario Ministry of Environment, Conservation and Parks (OMECP) at Toronto (orange) and Barrie (yellow), with a linear regression applied. The slope and R of each fit is given in the legend and the black line represents 1:1.

Table A1
For Each Defined Event, Air Quality Health Index (AQHI) Readings From Downtown Toronto, Indicating the Maximum Value Reached, the Number of Days Which Reached "Moderate Risk" and the Number of Days Which Reached "High Risk"

Event		Maximum AQHI	Number of days with moderate risk	# Of days with high risk
1	May 16–23, 2023	5	6	0
2	June 3–9, 2023	6	5	0
3	June 17–30, 2023	9	9	3

Table A2
Mean Summer (May-September) Values From the University of Toronto Atmospheric Observatory Fourier Transform Infrared (FTIR) spectrometer and Ontario Ministry of Environment, Conservation and Parks (OMECP) In Situ Instruments CO, O_3 and $PM_{2.5}$ Comparing the Previous Five Years (2018–2022) and 2023

Pollutant	Source	Five-year summer Mean (2018–2022)	2023 summer mean	Difference	2023 events mean	Difference
CO	TAO FTIR (10 km partial column)	1.80×10^{18} molec. cm^{-2}	2.28×10^{18} molec. cm^{-2}	27% higher	2.53×10^{18} molec. cm^{-2}	40% higher
	TOR. West OMECP (surface)	0.23 ppm	0.30 ppm	30% higher	0.32 ppm	39% higher
O_3	TAO FTIR (10 km partial column)	1.05×10^{18} molec. cm^{-2}	1.10×10^{18} molec. cm^{-2}	4% higher	1.22×10^{18} molec. cm^{-2}	16% higher
	TOR. DT. OMECP (surface)	27.9 ppb	31.4 ppb	12% higher	30.3 ppb	9% higher
	Barrie OMECP (surface)	25.9 ppb	26.4 ppb	2% higher	30.6 ppb	18% higher
$PM_{2.5}$	TOR. DT. OMECP (surface)	8.16 $\mu g/m^{-3}$	10.6 $\mu g/m^{-3}$	30% higher	16.5 $\mu g/m^{-3}$	202% higher
	Barrie OMECP (surface)	6.92 $\mu g/m^{-3}$	12.0 $\mu g/m^{-3}$	73% higher	21.0 $\mu g/m^{-3}$	303% higher

Table A3
Comparison Between Enhancement Ratios (Slope) and Respective R Values for the Events Individually (Figure 6) and Together (Figure A9)

	Slope				R-value			
Gas	Combined	Event 1	Event 2	Event 3	Combined	Event 1	Event 2	Event 3
C_2H_6	0.005	0.009	0.004	0.003	0.49	0.52	0.46	0.36
CH_3OH	0.017	0.028	0.016	0.021	0.79	0.82	0.64	0.87
HCN	0.003	0.006	0.003	0.003	0.65	0.52	0.51	0.77
HCOOH	0.013	0.030	0.012	0.013	0.67	0.86	0.66	0.87
NH_3	0.003	0.017	0.006	0.002	0.34	0.47	0.64	0.42
O_3	0.07	−0.199	−0.207	0.01	0.06	0.06	0.17	0.49

Note. The box is green if the slope/R value is higher for the event compared to the combined value, yellow if it is the same, and red if it is lower.

Acknowledgments
We acknowledge the support of the CSA Grant 21SUASABBC, led by PI Kaley Walker. The Toronto FTIR measurements were made at the University of Toronto Atmospheric Observatory and the Egbert FTIR measurements were made at the Centre for Atmospheric Research Experiments, with both primarily supported by the Natural Sciences and Engineering Research Council of Canada and Environment (NSERC) and ECCC. The EM27/SUNs are funded by the Canada Foundation for Innovation, the Ontario Research Fund, and ECCC. The MiniMPL is supported by NSERC, MPLNET, and MPLCAN. The MOPITT team acknowledges the contributions of COMDEV and ABB Bomem, with support from the CSA, NSERC, and ECCC. The NCAR MOPITT project is supported by the NASA Earth Observing System program. The authors gratefully acknowledge the NOAA Air Resources Laboratory for the provision of the HYSPLIT transport and dispersion model and the READY website (https://www.ready.noaa.gov) used in this publication. The model was run with National Centers for Environmental Prediction GDAS meteorology provided by the NOAA Physical Sciences Laboratory, Boulder, Colorado, USA, from their website at https://psl.noaa.gov. We thank Peter Englefield and the Canadian Forest Service for providing the active fire perimeters.

Data Availability Statement

The TAO FTIR data are publicly available in the NDACC data repository (NDACC, 2024). The OMECP surface measurements of $PM_{2.5}$, O_3 and CO, and AQHI readings are made available by the OMECP (OMECP, 2024). The GEM-MACH FireWork source code is made available by ECCC (Chen & GEM-MACH development team, 2019). The University of Toronto EM27/SUN total column XCO are archived online (Mostafavi et al., 2019). NASA provides open-source data for the MPLNET (NASA, 2024) and the MOPITT instrument (NASA/LARC/SD/ASDC, 2024). Burned area and polygon data are available at the Government of Canada—CWFIS Datamart (CWFIS, 2024).

References

Adams, C., McLinden, C. A., Shephard, M. W., Dickson, N., Dammers, E., Chen, J., et al. (2019). Satellite-derived emissions of carbon monoxide, ammonia, and nitrogen dioxide from the 2016 Horse River wildfire in the Fort McMurray area. *Atmospheric Chemistry and Physics*, *19*(4), 2577–2599. https://doi.org/10.5194/acp-19-2577-2019

Anderson, K., Chen, J., Englefield, P., Griffin, D., Makar, P., & Thompson, D. (2024). The Global Forest Fire Emissions Prediction System version 1.0. *Geoscientific Model Development*, *17*(21), 7713–7749. https://doi.org/10.5194/gmd-17-7713-2024

Campbell, J. R., Hlavka, D. L., Welton, E. J., Flynn, C. J., Turner, D. D., Spinhirne, J. D., et al. (2002). Full-time, eye-safe cloud and aerosol lidar observation at Atmospheric Radiation Measurement program sites: Instruments and data processing. *Journal of Atmospheric and Oceanic Technology*, *19*(4), 431–442. https://doi.org/10.1175/1520-0426(2002)019<0431:FTESCA>2.0.CO;2

Chen, J., & GEM-MACH development team. (2019). GEM-MACH CFFEPS rev m3848_CFFEPS (m3848_CFFEPS) [Software]. *Zenodo*. https://doi.org/10.5281/zenodo.2579386

Chen, J., Anderson, K., Pavlovic, R., Moran, M. D., Englefield, P., Thompson, D. K., et al. (2019). The FireWork v2.0 air quality forecast system with biomass burning emissions from the Canadian Forest Fire Emissions Prediction System v2.03. *Geoscientific Model Development*, *12*(7), 3283–3310. https://doi.org/10.5194/gmd-12-3283-2019

CWFIS (Canadian Wildland Fire Information System), Canadian Forest Service. (2024). Natural Resources Canada [Dataset]. *Northern Forestry Centre*. http://cwfis.cfs.nrcan.gc.ca

Deeter, M., Francis, G., Gille, J., Mao, D., Martínez-Alonso, S., Worden, H., et al. (2022). The MOPITT version 9 CO product: Sampling enhancements and validation. *Atmospheric Measurement Techniques*, *15*(8), 2325–2344. https://doi.org/10.5194/amt-15-2325-2022

De Mazière, M., Thompson, A. M., Kurylo, M. J., Wild, J. D., Bernhard, G., Blumenstock, T., et al. (2018). The Network for the Detection of Atmospheric Composition Change (NDACC): History, status and perspectives. *Atmospheric Chemistry and Physics*, *18*(7), 4935–4964. https://doi.org/10.5194/acp-18-4935-2018

Draxler, R. R. (2003). Evaluation of an ensemble dispersion calculation. *Journal of Applied Meteorology*, *42*(2), 308–317. https://doi.org/10.1175/1520-0450(2003)042<0308:EOAEDC>2.0.CO;2

Draxler, R. R., & Hess, G. D. (1998). An overview of the HYSPLIT4 modeling system for trajectories, dispersion, and deposition. *Australian Meteorological Magazine*, *47*, 295–308.

Draxler, R. R., & Rolph, G. D. (2007). HYSPLIT training seminar. Retrieved from https://www.arl.noaa.gov/documents/workshop/NAQC2007/HTML_Docs/index.html

Drummond, J. R., Bailak, G. V., & Mand, G. (1995). The Measurements of Pollution in the Troposphere (MOPITT) instrument. In G. A. Lampropoulos, J. Chrostowski, & R. M. Measures (Eds.), *Applications of photonic technology* (pp. 197–200). Springer US. https://doi.org/10.1007/978-1-4757-9247-8_38

ECCC (Environment and Climate Change Canada). (2024). Regional Air Quality Deterministic Prediction System (RAQDPS). Retrieved from https://collaboration.cmc.ec.gc.ca/cmc/CMOI/product_guide/docs/tech_notes/technote_raqdps_e.pdf

Esri. (2020). "Topographic" [basemap]. "OpenSteetMap". https://www.arcgis.com/home/item.html?id=b834a68d7a484c5fb473d4ba90d35e71

Esri. (2024). "Topographic" [basemap]. "Light Gray Canvas". https://www.arcgis.com/home/item.html?id=ee8678f599f64ec0a8ffbfd5c429c896

Farquhar, G. D., Firth, P. M., Wetselaar, R., & Weir, B. (1980). On the gaseous exchange of ammonia between leaves and the environment: Determination of the ammonia compensation point. *Plant Physiology*, *66*(4), 710–714. https://doi.org/10.1104/pp.66.4.710

Flood, V. A., Strong, K., Whaley, C. H., Walker, K. A., Blumenstock, T., Hannigan, J. W., et al. (2024). Evaluating modelled tropospheric columns of CH_4, CO, and O_3 in the Arctic using ground-based Fourier transform infrared (FTIR) measurements. *Atmospheric Chemistry and Physics*, *24*(2), 1079–1118. https://doi.org/10.5194/acp-24-1079-2024

Gisi, M., Hase, F., Dohe, S., Blumenstock, T., Simon, A., & Keens, A. (2012). XCO_2-measurements with a tabletop FTS using solar absorption spectroscopy. *Atmospheric Measurement Techniques*, *5*(11), 2969–2980. https://doi.org/10.5194/amt-5-2969-2012

Griffin, D., Sioris, C., Chen, J., Dickson, N., Kovachik, A., de Graaf, M., et al. (2020). The 2018 fire season in North America as seen by TROPOMI: Aerosol layer height intercomparisons and evaluation of model-derived plume heights. *Atmospheric Measurement Techniques*, *13*(3), 1427–1445. https://doi.org/10.5194/amt-13-1427-2020

Hanes, C. C., Wang, X., Jain, P., Parisien, M. A., Little, J. M., & Flannigan, M. D. (2019). Fire-regime changes in Canada over the last half century. *Canadian Journal of Forest Research*, *49*(3), 256–269. https://doi.org/10.1139/cjfr-2018-0293

Health Canada. (2023). *Guidance for Evaluating Human Health Effects in Impact Assessment: Air Quality. Healthy Environments and Consumer Safety Branch*, Health Canada. Retrieved from https://publications.gc.ca/collections/collection_2024/sc-hc/H129-54-1-2023-eng.pdf

Hedelius, J., & Wennberg, P. (2023). EM27/SUN GGG Interferogram processing suite (2020.0). *CaltechDATA*. https://doi.org/10.22002/25tve-4h822

IRWG (Infrared Working Group). (2020). Retrieval code SFIT – SFIT Spectral Data Analysis Model [Software]. https://wiki.ucar.edu/display/sfit4/

Jacob, D. J., Field, B. D., Li, Q., Blake, D. R., de Gouw, J., Warneke, C., et al. (2005). Global budget of methanol: Constraints from atmospheric observations. *Journal of Geophysical Research*, *110*(D8), D08303. https://doi.org/10.1029/2004JD005172

Jaffe, D. A., & Wigder, N. L. (2012). Ozone production from wildfires: A critical review. *Atmospheric Environment*, *51*, 1–10. https://doi.org/10.1016/j.atmosenv.2011.11.063

Jain, P., Barber, Q. E., Taylor, S., Whitman, E., Acuna, D. C., Boulanger, Y., et al. (2024). Drivers and impacts of the record-breaking 2023 wildfire season in Canada. *Nature Communications*, *15*, 6764. https://doi.org/10.1038/s41467-024-51154-7

Jones, M. W., Abatzoglou, J. T., Veraverbeke, S., Andela, N., Lasslop, G., Forkel, M., et al. (2022). Global and regional trends and drivers of fire under climate change. *Reviews of Geophysics*, *60*(3), e2020RG000726. https://doi.org/10.1029/2020RG000726

Kalnay, E., Kanamitsu, M., Kistler, R., Collins, W., Deaven, D., Gandin, L., et al. (1996). The NCEP/NCAR 40-year reanalysis project. *Bulletin of the American Meteorological Society*, *77*(3), 437–471. https://doi.org/10.1175/1520-0477(1996)077<0437:TNYRP>2.0.CO;2

Li, Y., Tong, D. Q., Ngan, F., Cohen, M. D., Stein, A. F., Kondragunta, S., et al. (2020). Ensemble $PM_{2.5}$ Forecasting during the 2018 camp fire event using the HYSPLIT transport and dispersion model. *Journal of Geophysical Research: Atmospheres*, *125*(15), e2020JD032768. https://doi.org/10.1029/2020JD032768

Lindaas, J., Pollack, I. B., Calahorrano, J. J., O'Dell, K., Garofalo, L. A., Pothier, M. A., et al. (2021). Empirical insights into the fate of ammonia in western US wildfire smoke plumes. *Journal of Geophysical Research: Atmospheres*, *126*(11), e2020JD033730. https://doi.org/10.1029/2020JD033730

Lolli, S., Vivone, G., Lewis, J. R., Sicard, M., Welton, E. J., Campbell, J. R., et al. (2020). Overview of the new version 3 NASA Micro-Pulse Lidar Network (MPLNET) automatic precipitation detection algorithm. *Remote Sensing*, *12*(1), 71. https://doi.org/10.3390/rs12010071

Lutsch, E., Dammers, E., Conway, S., & Strong, K. (2016). Long-range transport of NH_3, CO, HCN, and C_2H_6 from the 2014 Canadian wildfires. *Geophysical Research Letters*, *43*(15), 8286–8297. https://doi.org/10.1002/2016GL070114

Lutsch, E., Strong, K., Jones, D. B. A., Blumenstock, T., Conway, S., Fisher, J. A., et al. (2020). Detection and attribution of wildfire pollution in the Arctic and northern midlatitudes using a network of Fourier-transform infrared spectrometers and GEOS-Chem. *Atmospheric Chemistry and Physics*, *20*(21), 12813–12851. https://doi.org/10.5194/acp-20-12813-2020

Marsh, D. R., Mills, M. J., Kinnison, D. E., Lamarque, J.-F., Calvo, N., & Polvani, L. M. (2013). Climate change from 1850 to 2005 simulated in CESM1 (WACCM). *Journal of Climate*, *26*(19), 7372–7391. https://doi.org/10.1175/JCLI-D-12-00558.1

Matz, C. J., Egyed, M., Xi, G., Racine, J., Pavlovic, R., Rittmaster, R., et al. (2020). Health impact analysis of $PM_{2.5}$ from wildfire smoke in Canada (2013–2015, 2017–2018). *Science of the Total Environment*, *725*, 138506. https://doi.org/10.1016/j.scitotenv.2020.138506

Mendez-Espinosa, J. F., Belalcazar, L. C., & Morales Betancourt, R. (2019). Regional air quality impact of northern South America biomass burning emissions. *Atmospheric Environment*, *203*, 131–140. https://doi.org/10.1016/j.atmosenv.2019.01.042

Mostafavi, P., Nasrin, G., Lawson, Lu, G., Heerah, S., Hedelius, J., et al. (2019). Total column mixing ratios of carbon dioxide [Dataset]. *Methane and Carbon Monoxide from Toronto (ta). Borealis, V2*. https://doi.org/10.5683/SP2/RNCAWQ

NASA. (2024). MPLNET V3 data: Toronto downtown [Dataset]. https://mplnet.gsfc.nasa.gov/data?v=V3&s=Toronto_Downtown

NASA/LARC/SD/ASDC. (2024). MOPITT CO gridded daily means (Near and Thermal Infrared Radiances) V009 [Dataset]. *NASA Langley Atmospheric Science Data Center DAAC*. https://doi.org/10.5067/TERRA/MOPITT/MOP03J.009

NDACC. (2024). Network for the Detection of Atmospheric Composition Change [Dataset]. *NDACC Public Data Access*. https://www-air.larc.nasa.gov/missions/ndacc/data.html

NOAA (National Oceanic and Atmospheric Administration). (2024). National Centers for Environmental Information, Monthly Global Climate Report for Annual 2023. Retrieved from https://www.ncei.noaa.gov/access/monitoring/monthly-report/global/202313

OMECP (Ontario Ministry of Environment, Conservation and Parks). (2024). Air pollutant data [Dataset]. *Government of Ontario*. https://www.airqualityontario.com

Parisien, M. A., Barber, Q. E., Hirsch, K. G., Stockdale, C. A., Erni, S., Wang, X., et al. (2020). Fire deficit increases wildfire risk for many communities in the Canadian boreal forest. *Nature Communications*, *11*(1), 2121. https://doi.org/10.1038/s41467-020-15961-y

Paton-Walsh, C., Jones, N. B., Wilson, S. R., Haverd, V., Meier, A., Griffith, D. W. T., & Rinsland, C. P. (2005). Measurements of trace gas emissions from Australian forest fires and correlations with coincident measurements of aerosol optical depth. *Journal of Geophysical Research*, *110*(D24), 24305. https://doi.org/10.1029/2005JD006202

Paulot, F., Wunch, D., Crounse, J. D., Toon, G. C., Millet, D. B., DeCarlo, P. F., et al. (2011). Importance of secondary sources in the atmospheric budgets of formic and acetic acids. *Atmospheric Chemistry and Physics*, *11*(5), 1989–2013. https://doi.org/10.5194/acp-11-1989-2011

Pavlovic, R., Chen, J., Anderson, K., Moran, M. D., Beaulieu, P.-A., Davignon, D., & Cousineau, S. (2016). The FireWork air quality forecast system with near-real-time biomass burning emissions: Recent developments and evaluation of performance for the 2015 North American wildfire season. *Journal Air Waste Management*, *66*(9), 819–841. https://doi.org/10.1080/10962247.2016.1158214

Rodgers, C. D. (2000). Inverse methods for atmospheric sounding: Theory and practice. *World Scientific*, *2*, 13–100. https://doi.org/10.1142/3171

Rolph, G., Stein, A., & Stunder, B. (2017). Real-time Environmental Applications and Display sYstem: READY. *Environmental Modelling & Software*, *95*, 210–228. https://doi.org/10.1016/j.envsoft.2017.06.025

Rothman, L. S., Gordon, I. E., Barbe, A., Benner, D. C., Bernath, P. F., Birk, M., et al. (2009). The HITRAN 2008 molecular spectroscopic database. *Journal of Quantitative Spectroscopy and Radiative Transfer*, *110*(9–10), 533–572. https://doi.org/10.1016/j.jqsrt.2009.02.013

Schneider, S. R., Lee, K., Santos, G., & Abbatt, J. P. (2021). Air quality data approach for defining wildfire influence: Impacts on $PM_{2.5}$, NO_2, CO, and O_3 in Western Canadian cities. *Environmental Science and Technology*, *55*(20), 13709–13717. https://doi.org/10.1021/acs.est.1c04042

Selimovic, V., Yokelson, R. J., McMeeking, G. R., & Coefield, S. (2019). In situ measurements of trace gases, PM, and aerosol optical properties during the 2017 NW US wildfire smoke event. *Atmospheric Chemistry and Physics*, *19*(6), 3905–3926. https://doi.org/10.5194/acp-19-3905-2019

Statistics Canada. (2023). Census Profile, 2021 Census of Population. *Statistics Canada Catalogue number 98-316-X2021001*. Retrieved from https://www12.statcan.gc.ca/census-recensement/2021/dp-pd/prof/index.cfm?Lang=E

Stein, A. F., Draxler, R. R., Rolph, G. D., Stunder, B. J. B., Cohen, M. D., & Ngan, F. (2015). NOAA's HYSPLIT atmospheric transport and dispersion modeling system. *Bulletin of the American Meteorological Society*, *96*(12), 2059–2077. https://doi.org/10.1175/BAMS-D-14-00110.1

Stein, A. F., Rolph, G. D., Draxler, R. R., Stunder, B., & Ruminski, M. (2009). Verification of the NOAA smoke forecasting system: Model sensitivity to the injection height. *Weather and Forecasting*, *24*(2), 379–394. https://doi.org/10.1175/2008WAF2222166.1

Teledyne Advanced Pollution Instrumentation. (2016). Model T640 PM Mass Monitor User Manual. Retrieved from https://www.teledyne-api.com/prod/Downloads/08354C%20T640%20USER%20MANUAL.pdf

Thermo Fisher Scientific. (2013). Model 5030 Synchronized Hybrid Ambient Real-time Particulate Monitor Instruction Manual. Retrieved from https://tools.thermofisher.com/content/sfs/manuals/EPM-manual-Model%205030%20SHARP.pdf

Thermo Fisher Scientific. (2017a). Model 48i Gas Filter Correlation CO Analyzer Instruction Manual. Retrieved from https://assets.thermofisher.com/TFS-Assets/LSG/manuals/48i_101891-00_10Aug2017.pdf

Thermo Fisher Scientific. (2017b). Model 49i UV Photometric O3 Analyzer Instruction Manual. Retrieved from https://assets.thermofisher.com/TFS-Assets/EPM/manuals/EPM-manual-Model%2049i.pdf

Tomsche, L., Piel, F., Mikoviny, T., Nielsen, C. J., Guo, H., Campuzano-Jost, P., et al. (2023). Measurement report: Emission factors of NH_3 and NH_x for wildfires and agricultural fires in the United States. *Atmospheric Chemistry and Physics*, *23*(4), 2331–2343. https://doi.org/10.5194/acp-23-2331-2023

USFS (United States Forest Service). (2024). Ensemble - Wildland Fire Air Quality Tools. Retrieved from https://portal.airfire.org/

Van Wagner, C. E. (1987). Development and structure of the Canadian forest fire weather index system. *Forestry Technical Report*, *35*, 35. Retrieved from https://cfs.nrcan.gc.ca/publications?id=19927

Viatte, C., Strong, K., Paton-Walsh, C., Mendonca, J., O'Neill, N. T., & Drummond, J. R. (2013). Measurements of CO, HCN, and C_2H_6 total columns in smoke plumes transported from the 2010 Russian boreal forest fires to the Canadian high Arctic. *Atmosphere-Ocean*, *51*(5), 522–531. https://doi.org/10.1080/07055900.2013.823373

Vigouroux, C., Hendrick, F., Stavrakou, T., Dils, B., De Smedt, I., Hermans, C., et al. (2009). Ground-based FTIR and MAX-DOAS observations of formaldehyde at Réunion Island and comparisons with satellite and model data. *Atmospheric Chemistry and Physics*, *9*(24), 9523–9544. https://doi.org/10.5194/acp-9-9523-2009

Wentworth, G. R., Aklilu, Y.-A., Landis, M. S., & Hsu, Y.-M. (2018). Impacts of a large boreal wildfire on ground level atmospheric concentrations of PAHs, VOCs and ozone. *Atmospheric Environment*, *178*, 19–30. https://doi.org/10.1016/j.atmosenv.2018.01.013

Whaley, C., Strong, K., Adams, C., Bourassa, A. E., Daffer, W. H., Degenstein, D. A., et al. (2013). Using FTIR measurements of stratospheric composition to identify midlatitude polar vortex intrusions over Toronto. *Journal of Geophysical Research: Atmospheres*, *118*(22), 12766–12783. https://doi.org/10.1002/2013JD020577

Whaley, C. H., Makar, P. A., Shephard, M. W., Zhang, L., Zhang, J., Zheng, Q., et al. (2018). Contributions of natural and anthropogenic sources to ambient ammonia in the Athabasca Oil Sands and north-western Canada. *Atmospheric Chemistry and Physics*, *18*(3), 2011–2034. https://doi.org/10.5194/acp-18-2011-2018

Wizenberg, T., Strong, K., Jones, D. B. A., Lutsch, E., Mahieu, E., Franco, B., & Clarisse, L. (2023). Exceptional wildfire enhancements of PAN, C_2H_4, CH_3OH, and HCOOH over the Canadian high Arctic during August 2017. *Journal of Geophysical Research: Atmospheres*, *128*(10), e2022JD038052. https://doi.org/10.1029/2022JD038052

Xiao, Y., Logan, J. A., Jacob, D. J., Hudman, R. C., Yantosca, R., & Blake, D. R. (2008). Global budget of ethane and regional constraints on US sources. *Journal of Geophysical Research*, *113*(D21), D21306. https://doi.org/10.1029/2007JD009415

Yamanouchi, S., Conway, S., Strong, K., Colebatch, O., Lutsch, E., Roche, S., et al. (2023). Network for the Detection of Atmospheric Composition Change (NDACC) Fourier transform infrared (FTIR) trace gas measurements at the University of Toronto Atmospheric Observatory from 2002 to 2020. *Earth System Science Data*, *15*(8), 3387–3418. https://doi.org/10.5194/essd-15-3387-2023

Yamanouchi, S., Strong, K., Lutsch, E., & Jones, D. B. A. (2020). Detection of HCOOH, CH_3OH, CO, HCN, and C_2H_6 in Wildfire Plumes Transported over Toronto using ground-based FTIR measurements from 2002–2018. *Journal of Geophysical Research: Atmospheres*, *125*(16), e2019JD031924. https://doi.org/10.1029/2019JD031924

York, D., Evensen, N. M., Martínez, M. L., & De Basabe Delgado, J. (2004). Unified equations for the slope, intercept, and standard errors of the best straight line. *American Journal of Physics*, *72*(3), 367–375. https://doi.org/10.1119/1.1632486

Zhang, S., Solomon, S., Boone, C. D., & Taha, G. (2024). Investigating the vertical extent of the 2023 summer Canadian wildfire impacts with satellite observations. *Atmospheric Chemistry and Physics*, *24*(20), 11727–11736. https://doi.org/10.5194/acp-24-11727-2024